

---

# Climate Data Record (CDR) Program

## Climate Algorithm Theoretical Basis Document (C-ATBD)

### Total Solar Irradiance and Solar Spectral Irradiance



CDR Program Document Number: CDRP-ATBD-0612  
Configuration Item Number: 01B-32, 01B-33  
Revision 1 / April 7, 2015

**REVISION HISTORY**

<b>Rev.</b>	<b>Author</b>	<b>DSR No.</b>	<b>Description</b>	<b>Date</b>
1	Odele Coddington, LASP Judith Lean, NRL	DSR-788	Initial Submission to CDR Program	04/07/2015

## TABLE of CONTENTS

<b>1. INTRODUCTION.....</b>	<b>1</b>
1.1 Purpose .....	1
1.2 Definitions.....	1
1.3 Document Maintenance.....	1
<b>2. OVERVIEW OF SOLAR IRRADIANCE CLIMATE DATA RECORD .....</b>	<b>3</b>
2.1 Products Generated .....	3
2.2 Instrument and Model Characteristics .....	3
<b>3. ALGORITHM DESCRIPTION.....</b>	<b>5</b>
3.1 Algorithm Overview .....	5
3.2 Processing Outline.....	5
3.3 Algorithm Input.....	7
3.3.1 Primary Input Data .....	7
3.3.2 Ancillary Data.....	9
3.3.3 Derived Data .....	9
3.3.4 Forward Models.....	10
3.4 Theoretical Description .....	10
3.4.1 Physical and Mathematical Description .....	16
3.4.2 Data Merging Strategy.....	19
3.4.3 Numerical Strategy .....	19
3.4.4 Calculations.....	19
3.4.5 Look-Up Table Description .....	20
3.4.6 Parameterization .....	20
3.4.7 Algorithm Output.....	20
<b>4. TEST DATASETS AND OUTPUTS.....</b>	<b>23</b>
4.1 Test Input Datasets .....	23
4.2 Test Output Analysis .....	24
4.2.1 Reproducibility.....	24
4.2.2 Precision and Accuracy .....	24
4.2.3 Error Budget .....	25
<b>5. PRACTICAL CONSIDERATIONS.....</b>	<b>33</b>
5.1 Numerical Computation Considerations.....	33
5.2 Programming and Procedural Considerations .....	33
5.3 Quality Assessment and Diagnostics .....	33
5.4 Exception Handling.....	34
5.5 Algorithm Validation .....	34
5.6 Processing Environment and Resources .....	36
<b>6. ASSUMPTIONS AND LIMITATIONS .....</b>	<b>37</b>

**6.1 Algorithm Performance ..... 39**

**6.2 Sensor Performance ..... 40**

**7. FUTURE ENHANCEMENTS..... 42**

**7.1 Enhancement 1 ..... 42**

**7.2 Enhancement 2 ..... 43**

**7.3 Enhancement 3 ..... 44**

**8. REFERENCES..... 46**

**APPENDIX A. ACRONYMS AND ABBREVIATIONS ..... 49**

## LIST of FIGURES

Figure 1: Flow diagram of the algorithm processing.

Figure 2: Facular brightening and sunspot darkening time series variations during the solar cycle, input to the algorithm.

Figure 3: Facular brightening and sunspot darkening time series variations during solar rotation, input to the algorithm.

Figure 4: Reference spectrum of the quiet Sun adopted for the NRLSSI2 irradiance variability model used in the algorithm (upper) and comparisons with other spectra (lower).

Figure 5: Scaling coefficients that the algorithm uses to convert the facular brightening and sunspot darkening indices in Figures 2 and 3 to their equivalent irradiance change, in energy units.

Figure 6: Total solar irradiance reconstructed with the NRLSSI2 model algorithm (upper), and the corresponding individual facular and sunspot contributions to total solar irradiance variations (lower).

Figure 7: Solar spectral irradiance variations calculated by the NRLSSI2 model algorithm during recent solar cycles and binned in four broad wavelength bands.

Figure 8: Comparison of NRLSSI2 total irradiance variations calculated by the algorithm, with the integral of the NRLSSI2 spectra also calculated by the algorithm (upper) and similar comparisons of their respective facular and sunspot components (lower).

Figure 9: Comparison of NRLSSI2 total solar irradiance variations calculated by the algorithm with an earlier model, NRLSSI.

Figure 10: Comparisons of NRLSSI2 solar spectral irradiance variation calculated by the algorithm and binned in selected broad wavelength bands, as shown in Figure 7, with an earlier model, NRLSSI. On the left are the time series in energy units and on the right are percentage differences.

Figure 11. Examples of NRLSSI2 total solar irradiance variations and estimated uncertainties in the relative changes (i.e., excluding the  $\pm 0.5 \text{ W m}^{-2}$  uncertainty in the total solar irradiance absolute scale) that the algorithm calculates during epochs of high solar activity (left) and moderate solar activity (right).

Figure 12. Percentage uncertainties in the NRLSSI2 modeled solar spectral irradiance change on 30<sup>th</sup> October 2003 (a time of relatively high solar activity) relative to the spectral irradiance of the quiet sun (i.e., excluding the uncertainty of the spectral solar irradiance absolute scale) calculated by the algorithm.

Figure 13. Solar spectral irradiance variations calculated by the algorithm are shown for the four wavelengths listed in Table 6, with estimated uncertainties in the relative changes (i.e., excluding the uncertainty of the total solar irradiance absolute scale) during an epoch of relatively high solar activity.

Figure 14: The total solar irradiance time series calculated by the algorithm (NRLTSI2 model) is compared with TIM observations during solar rotation (upper panel) and during the solar cycle (middle and lower panels).

Figure 15: Differences in daily total solar irradiance that the algorithm calculates (according to NRLTSI2) with TIM observations (upper) and the original NRLTSI model (lower).

Figure 16: Shown are time series of solar spectral irradiance variations that the algorithm calculates (i.e., the NRLSSI2 model) and binned in broad wavelength bands compared with SIM observations from 2003 to 2005. The primary variations are associated with the Sun's 27-day rotation.

Figure 17: Shown are the solar spectral irradiance changes during solar cycle 24, in both percentages (upper) and energy units (lower), that the algorithm calculates (using the NRLSSI2 model) from solar minimum at the end of 2008 to near solar maximum at the beginning of 2013, compared with corresponding changes estimated using the original NRLSSI model.

## LIST of TABLES

Table 1: Definitions of symbols used in the C-ATBD.

Table 2: Solar irradiance products that this CDR provides.

Table 3: Structure of the algorithm (NRLTSI2) output for daily values of total solar irradiance (TSI) from 1978 to the present.

Table 4: Structure of the algorithm (NRLSSI2) output for daily values of solar spectral irradiance (SSI) from 1978 to the present.

Table 5: Representative quantities and their uncertainties, used to estimate  $1-\sigma$  relative uncertainties in the daily value of total solar irradiance produced by the algorithm on 30th October 2003, when facular brightening and sunspot darkening values were relatively high. Note that  $FQ=0.1502$  and  $SQ = 0$ .

Table 6: Representative quantities and their uncertainties, used to estimate  $1-\sigma$  relative uncertainties in daily values of solar spectral irradiance produced by the algorithm on 30th October 2003, when facular brightening and sunspot darkening values were relatively high.

Table 7: Summary of assumptions in the theoretical basis for the algorithm's calculations of solar irradiance variability, algorithm inputs and the potential validation approaches.

# 1. Introduction

## 1.1 Purpose

The purpose of this document is to describe the algorithm submitted to the National Climatic Data Center (NCDC) by Judith Lean (Space Science Division, Naval Research Laboratory), Odele Coddington and Peter Pilewski (Laboratory for Atmospheric and Space Physics, University of Colorado) that is used to create the Total Solar Irradiance and Solar Spectral Irradiance Climate Data Records (CDR). Also described are the solar activity indices of sunspot darkening,  $S(t)$ , and facular brightening,  $F(t)$ , that are input to the algorithm. The algorithm's calculations of solar irradiance augment direct measurements made by the Total and Spectral Solar Irradiance Sensor (TSIS). The actual algorithm is defined by the computer program (code) that accompanies this document; this C-ATBD provides a guide to understanding that algorithm, from both a scientific perspective and in order to assist a software engineer or end-user performing an evaluation of the code.

This C-ATBD describes the procedures, algorithms and input datasets used to construct the total solar irradiance and the concurrent solar spectral irradiance variations during recent decades and in historical time periods since 1610. Also described are the output files of daily, monthly and annual solar irradiance, and validation procedures for the modeled solar irradiance. The solar irradiance reconstructions that this C-ATBD describes complement the direct measurements made of total and spectral solar irradiance by the TSIS instrument, documented in the separate TSIS ATBD.

## 1.2 Definitions

Table 1 provides definitions of symbols used in this C-ATBD.

## 1.3 Document Maintenance

The algorithm that calculates the total solar irradiance (TSI) and solar spectral irradiance (SSI) that compose the Solar Irradiance Climate Data Record uses bolometric (for TSI) and wavelength-dependent (for SSI) coefficients to convert two time-varying inputs, the facular brightening index,  $F(t)$ , and the sunspot darkening index,  $S(t)$ , into their respective modulations of the solar irradiance of the "quiet" Sun (i.e., in the absence of these activity features). The starting point for the algorithm is a baseline (invariant) value of total,  $T_Q$ , and spectral,  $I_Q(\lambda)$ , irradiance representative of the "quiet" (inactive) Sun, obtained directly from space-based irradiance observations. The numerical values of the coefficients that determine the irradiance modulation imposed by sunspots and faculae, when these features are present on the solar disk, are determined from analysis of variability in extant TSI and SSI datasets measured by instruments onboard the Solar Radiation and Climate (SORCE) spacecraft (Rottman et al., 2005). Neither the baseline irradiance values nor the coefficients that calculate the irradiance modulation with time are expected to change on time scales shorter than a few years, which is the time frame over which new information can be expected to accrue from ongoing TSIS

measurements. For this reason, it is not expected that the algorithm will evolve rapidly, nor that frequent synchronization will be needed.

**Table 1. Definitions of symbols used in the C-ATBD.**

Symbol	Definition	Units
t	time	day, month, year
$\lambda$	wavelength	nm
T(t)	total solar irradiance at time t	$\text{W m}^{-2}$
$T_Q$	total solar irradiance (TSI) of the quiet (inactive) Sun; invariant with time	$\text{W m}^{-2}$
$I(\lambda, t)$	solar spectral irradiance (SSI) at wavelength $\lambda$ and time t	$\text{W m}^{-2} \text{ nm}^{-1}$
$I_Q(\lambda)$	solar spectral irradiance of the quiet (inactive) Sun at wavelength $\lambda$	$\text{W m}^{-2} \text{ nm}^{-1}$
F(t)	facular brightening index at time t	units of the SCIAMACHY Mg index
S(t)	sunspot darkening index at time t	millionths of solar hemisphere
$F_Q$	facular brightening of the quiet (invariant) Sun, corresponding to $I_Q$ and $S_Q$	units of the SCIAMACHY Mg index
$S_Q$	sunspot darkening of the quiet (invariant) Sun, corresponding to $I_Q$ and $F_Q$	millionths of solar hemisphere
$A_S$	sunspot area	millionths of solar hemisphere
$\mu$	sunspot location in radial heliocentric coordinates	
Mg(t)	The Mg II index at time t, determined as the ratio of core to wing emission in the Mg II Fraunhofer line	units of the SCIAMACHY Mg index

## 2. Overview of Solar Irradiance Climate Data Record

### 2.1 Products Generated

The Solar Irradiance Climate Data Record provides values of the total and spectral irradiance as functions of time, listed in Table 2. Total solar irradiance,  $T(t)$ , is the total, spectrally integrated (i.e., bolometric) energy input to the top of the Earth's atmosphere, at a standard (invariant) distance of one Astronomical Unit (1AU) from the Sun. Its units are  $\text{W m}^{-2}$ . Solar Spectral Irradiance,  $I(\lambda, t)$ , is the corresponding spectrum that integrates self-consistently to the total. Values of solar spectral irradiance are provided in 3785 (variable width) wavelength bands from  $115.5 \pm 0.5 \text{ nm}$  to  $99,975 \pm 25 \text{ nm}$ , in units of  $\text{W m}^{-2} \text{ nm}^{-1}$ .

Both direct observations and model calculations contribute to the Solar Irradiance Climate Data record. The Total and Spectral Irradiance Sensor (TSIS) is the corresponding observing system that measures the total solar irradiance and solar spectral irradiance directly. It is described in a separate ATBD (Coddington et al., 2013). The Naval Research Laboratory Total Solar irradiance (NRLTSI2) and Naval Research Laboratory Solar Spectral irradiance (NRLSSI2) models, developed from the SORCE database of solar irradiance observations, calculate the irradiance from two primary (time varying) inputs, the facular brightening,  $F(t)$ , and sunspot darkening,  $S(t)$ .

Also provided are five reference spectra indicative of quiet, low, moderate and high solar activity levels, and the Maunder Minimum, in 99844 bins of equal 1 nm width, from 115.5 to 99999.5 nm.

### 2.2 Instrument and Model Characteristics

The primary solar irradiance observational dataset for the Solar Irradiance Climate Data Record is that measured by the Total and Spectral Solar Irradiance Sensor (TSIS), which a separate ATBD document describes (Coddington et al., 2013).

The present document describes the algorithm that calculates total solar irradiance and solar spectral irradiance using the NRLTSI2 and NRLSSI2 models, respectively, developed from direct solar irradiance observations made by the Total Irradiance Monitor (TIM) and Solar Irradiance Monitor (SIM) on the Solar Radiation and Climate Experiment (SORCE) spacecraft from 2003 to 2014. The NRLTSI2 and NRLSSI2 models are the second generation of the NRLTSI and NRLSSI solar irradiance variability models that input proxy indicators of faculae and sunspots to calculate the change in a reference spectrum that these features produce, when present on the solar disc. Lean and Woods (2010) provide an overview of the NRLTSI and NRLSSI models.

The total solar irradiance generated by the NRLTSI2 model is directly comparable with daily average values of the total solar irradiance measured by the next-generation TIM, which is part of TSIS. The solar spectral irradiance generated by the NRLSSI2 model is directly comparable with daily average values of the next-generation SIM, which is also part of TSIS, after adjustment to match the wavelength bins on which the TSIS SIM measurements are reported. The SIM has a single dispersive optical element, a prism, and the spectral resolution is a strong

function of wavelength related to the geometry of the prism and the optical dispersion of the fused silica prism material (Coddington et al., 2013). The measured spectra are therefore interpolated onto 1 nm wavelength bins for the development of the NRLSSI2 model coefficients and for comparison against the modeled data.

**Table 2. Solar irradiance products that this CDR provides.**

<b>Product</b>	<b>Type</b>	<b>Number of Wavelength Bins</b>	<b>Time Range</b>	<b>Cadence</b>
Total Solar Irradiance	Observational composite	1	1978-2014	Daily, single file: no update cadence
Total Solar Irradiance	NRLTSI2 model	1	1882-2014	Daily, monthly files: quarterly updates
Total Solar Irradiance	NRLTSI2 model	1	1610-2014	Annual files: yearly update
Solar Spectral Irradiance	NRLSSI2 model	3785 (variable width)	1882-2014	Daily, monthly files: quarterly updates
Solar Spectral Irradiance	NRLSSI2 model	3785 (variable width)	1610-2014	Annual files: yearly update
Solar Spectral Irradiance	Reference Spectrum	99884 (1 nm width)	Quiet, low, moderate and high solar activity	Four individual reference spectra representative of minimum (Quiet) Sun conditions, low, moderate and high solar activity single files: no update cadence
Solar Spectral Irradiance	NRLSSI2 model spectrum	99884 (1 nm width)	Maunder Minimum (estimated)	Single, modeled, spectrum representative of Maunder minimum Sun activity, single file: no update cadence
Facular brightening and sunspot darkening indices	NRLTSI2 and NRLSSI2 inputs	N/A	1882 – 2014	Daily, monthly files: quarterly update

## 3. Algorithm Description

### 3.1 Algorithm Overview

The Solar Irradiance Data Record algorithm uses the NRLTSI2 and NRLSSI2 models to calculate values of the total irradiance and the solar spectral irradiance in 3,785 (variable) wavelength bins (on a wavelength grid from 115.5 to 99975 nm) when supplied with two inputs; the facular brightening,  $F(t)$ , and sunspot darkening,  $S(t)$ , indices, each of which varies with time,  $t$ .

The facular and sunspot influences on solar irradiance are calculated in  $\text{W m}^{-2}$  by applying (constant) scaling coefficients to the input facular and sunspot indices, and the resultant irradiance increments are then applied to adjust the specified (invariant) baseline total irradiance and spectral irradiance which indicate the “quiet” sun (see Table 2) Lean (2000) describes the basic approach and Lean et al. (2005) update the approach and compare modeled solar irradiance variability modeled with early SORCE observations. For the purposes of the algorithm, the quiet sun irradiance is that corresponding to the absence of both sunspots and faculae.

When applying the model formulation to estimate plausible historical solar irradiance variations for use in climate change research, an additional third component is introduced to estimate the hypothesized (e.g., Lean et al., 1992; Lean et al., 2005) contribution of a long-term facular component that produces secular irradiance change underlying the solar activity cycle on multi-decadal time scales (prior to 1950), since 1610, including during the Maunder Minimum of anomalously low solar activity.

Table 2 summarizes the outputs of the algorithm.

### 3.2 Processing Outline

The flow diagram in Figure 1 provides an overview of algorithm processing steps in calculating the total solar irradiance,  $T(t)$ , and solar spectral irradiance,  $I(\lambda, t)$ , at a specified time,  $t$ . The algorithm assumes that when faculae and sunspots are present on the solar disc, they alter the baseline (quiet) total solar irradiance,  $T_Q$ , by amounts  $\Delta T_F(t)$  and  $\Delta T_S(t)$ , respectively, so that:

$$T(t) = T_Q + \Delta T_F(t) + \Delta T_S(t)$$

Similarly the faculae and sunspots alter the baseline solar spectral irradiance,  $I_Q(\lambda)$ , by wavelength-dependent amounts,  $\Delta I_F(\lambda, t)$  and  $\Delta I_S(\lambda, t)$ , so that

$$I(\lambda, t) = I_Q(\lambda) + \Delta I_F(\lambda, t) + \Delta I_S(\lambda, t)$$

where the integrated spectral irradiance equals the corresponding total irradiance:

$$T(t) = \int_{\lambda_0}^{\lambda_\infty} I(\lambda, t) d\lambda$$

$$T_Q = \int_{\lambda_0}^{\lambda_\infty} I_Q(\lambda) d\lambda$$

The first step in the algorithm is determination of the corresponding values for the facular brightening,  $F(t)$ , and sunspot darkening,  $S(t)$ , indices at time,  $t$ , which produce incremental changes in total solar irradiance:

$$\Delta T_F(t) \propto F(t)$$

$$\Delta T_S(t) \propto S(t)$$

and in solar spectral irradiance:

$$\Delta I_F(\lambda, t) \propto F(t)$$

$$\Delta I_S(\lambda, t) \propto S(t)$$

such that

$$\Delta T_F(t) = \int_{\lambda_0}^{\lambda_\infty} \Delta I_F(\lambda, t) d\lambda$$

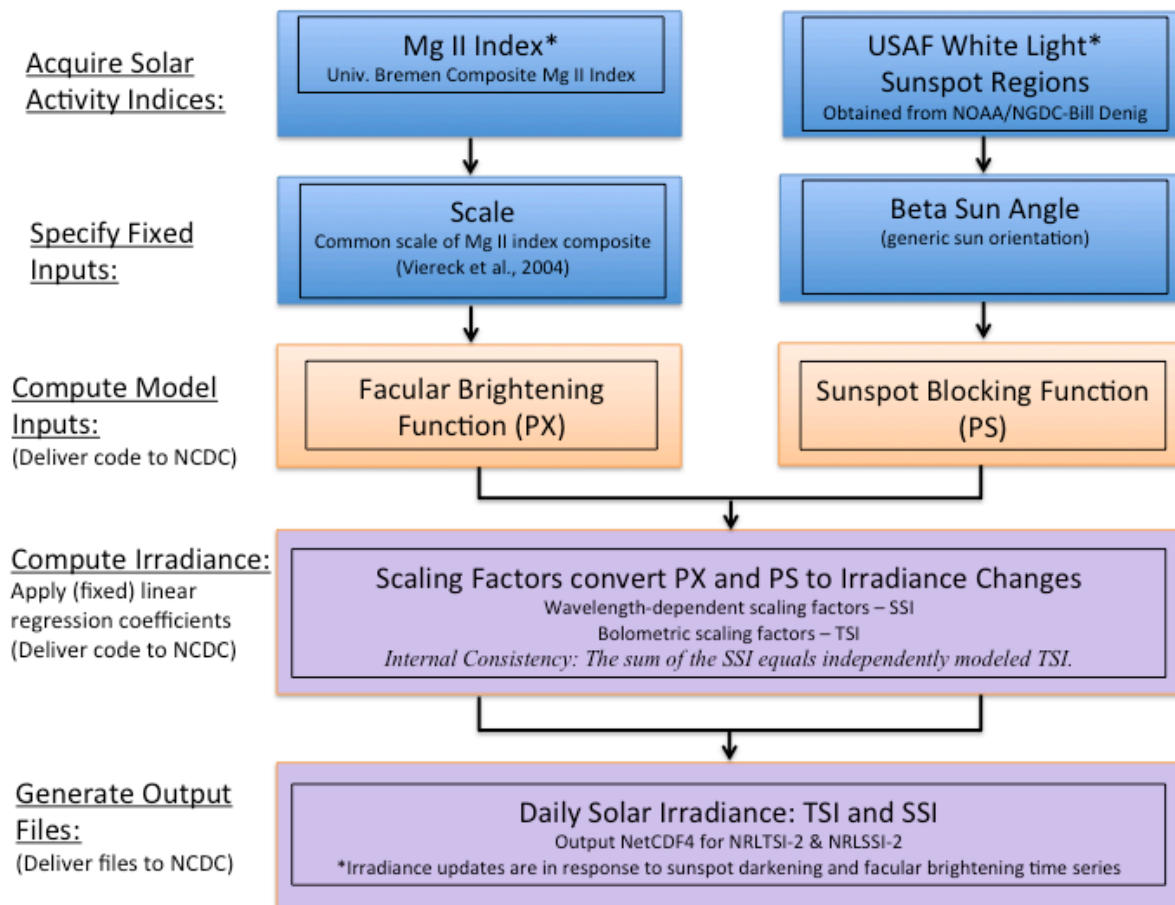
$$\Delta T_S(t) = \int_{\lambda_0}^{\lambda_\infty} \Delta I_S(\lambda, t) d\lambda$$

The facular brightening index is obtained by downloading the space-based Mg II composite (hereafter, the University of Bremen Composite Mg II index) index of solar activity constructed by combining observations made by the GOME, SCIAMACHY and GOME-2 instruments (see Snow et al., 2014 for composite details), available at <http://www.iup.uni-bremen.de/UVSAT/Datasets/mgii>. The sunspot darkening index is obtained from data downloaded from NOAA NGDC, in the form of annual files of active region information compiled from the Air Force Solar Observing Optical Network (SOON) sites. The link is <http://www.ngdc.noaa.gov/stp/spaceweather.html>, ftp access, Solar\_Data, Sunspot\_Regions, USAF\_MWL. The files provide information about the areas,  $A_S$ , and locations,  $\mu$ , of individual sunspot active regions present on the solar disk on any given day.

Adding the total and spectral irradiance increments due to faculae and sunspots to the baseline reference total solar irradiance and solar spectral irradiance then determines the total and spectral irradiance at time,  $t$ . Values of the (invariant) total and spectral irradiance of the quiet Sun,  $T_Q$  and  $I_Q(\lambda)$ , are specified in the algorithm code as baseline references for this purpose. Solar spectral irradiance is initially estimated on a uniform wavelength grid, on 0.5 nm centers, in 1 nm bins from 115.5 to 99999.5 nm, which is also the wavelength grid of the reference spectrum. The spectral irradiance is then averaged (i.e. the binned spectral irradiance is normalized by the spectral band width) into 3785 wavelength bins of variable width, designed appropriately for input to general circulation climate models.

Output files are generated separately for total solar irradiance and solar spectral irradiance. The TSI is one value per input facular brightening and sunspot darkening index values, typically daily. The units are  $\text{W m}^{-2}$ . The SSI is one spectrum per input facular brightening and sunspot darkening index values, also typically daily. The solar spectral irradiance is produced in 3785 wavelengths binds, in units of  $\text{W m}^{-2} \text{nm}^{-1}$ .

**Figure 1. Flow diagram of the algorithm processing.**



### 3.3 Algorithm Input

#### 3.3.1 Primary Input Data

Adopted for the facular brightening index,  $F(t)$ , is the global (disk-integrated) Mg II emission from the Sun's chromosphere, whose variations are dominated by chromospheric extensions of photospheric faculae. The Mg II index (which is the ratio of core emission in Fraunhofer lines to emission in the nearby continuum) is such a proxy because the core emission is enhanced in magnetically active bright regions, and the indices are sensitive indicators of the total (net) emission from all bright regions on the solar disk (Skupin et al., 2004; Snow et al., 2005). Furthermore, as the ratio of absolute fluxes, the Mg II index is (in principle) less susceptible to

instrumental sensitivity changes that potentially contaminate the temporal fidelity of the facular index time series.

The sunspot darkening index,  $S(t)$ , is calculated following Lean et al. (1998) using direct observations of the areas,  $A_S$ , and heliocentric locations,  $\mu$ , of  $N_{spot}$  individual sunspot regions that the Air Force SOON (and other ground- and space-based) sites observe daily. The calculation effectively sums the projected area of sunspot regions on the solar hemisphere and multiplies this by the contrast of sunspots relative to the background (reference) Sun, taking into account variations with limb position on the solar disk. Areas prior to 1976 are reduced by 20% to account for systematic area differences between Greenwich and Air Force SOON measurements.

Summing over all sunspots, the sunspot darkening index is

$$S(t) = 0.32 \sum_1^{N_{spot}} A_S \left( \frac{3\mu+2}{2} \right) \mu$$

where  $\mu = \cos(\text{latitude}) \times \cos(\text{longitude})$  for spot latitude (adjusted for the  $B_0$  angle of the Sun's axis to the ecliptic plane) and longitude in heliocentric coordinates.

Figure 2 shows time series of the facular brightening and sunspot darkening indices since 1978, illustrating their evolution during the solar cycle as active regions emerge, evolve, and disappear from the solar disk. Figure 3 shows variations of these indices during 2003-2004, illustrating their shorter-term modulation arising from solar rotation. The facular brightening,  $F(t)$ , and sunspot darkening,  $S(t)$ , time-varying inputs that the Solar Irradiance Climate Data Record algorithm uses to calculate solar irradiance must be carefully calculated and validated, with possible erroneous values flagged for investigation (see Table 7). For this purpose, both the facular and sunspot indices are routinely compared with various related but independent solar records including the Call K facular brightening index measured by the Sacramento Peak Observatory ([http://nsosp.nso.edu/cak\\_mon](http://nsosp.nso.edu/cak_mon)) and the sunspot darkening index calculated from observations made at the Debrecen Solar Observatory ([http://fenyi.solarobs.unideb.hu/deb\\_obs\\_en.html](http://fenyi.solarobs.unideb.hu/deb_obs_en.html)).

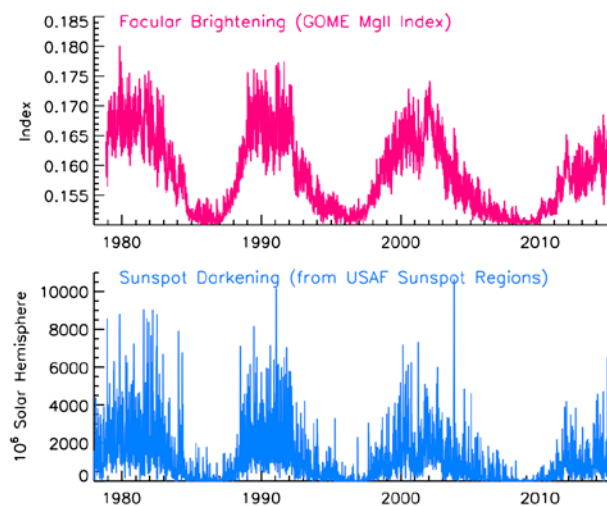


**Figure 2. Facular brightening and sunspot darkening time series variations during the solar cycle, input to the algorithm.**

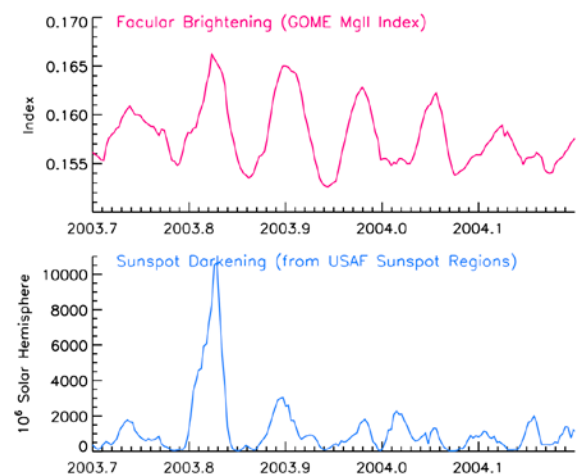


**Figure 3. Facular brightening and sunspot darkening time series variations during solar rotation, input to the algorithm.**

### 3.3.2 Ancillary Data

The algorithm uses constant baseline values of the total solar irradiance,  $T_Q$ , and solar spectral irradiance,  $I_Q(\lambda)$ , to represent the quiet sun, as shown in Figure 4. The adopted baseline total solar irradiance is  $T_Q = 1360.45 \text{ Wm}^{-2}$ , which is consistent with the value of  $1360.8 \pm 0.5 \text{ Wm}^{-2}$  that Kopp and Lean (2011) report from direct observations made by TIM on SORCE. Adopted for the corresponding solar spectral irradiance of the quiet sun (on a 1 nm wavelength grid), is the Whole Heliosphere Interval (WHI) reference spectrum compiled from SORCE observations (Woods et al., 2009) at wavelengths less than 300 nm, the SOLSPEC spectrum (which has higher spectral resolution than that of SORCE measurements, Thuillier et al., 1998) for wavelengths from 300 to ~2000 nm (adjusted to the overall shape of the WHI reference spectrum), and the theoretical spectrum of Kurucz (1991) at longer wavelengths, adjusted to make the integrated energy of the quiet solar spectrum equal that of total solar irradiance. Figure 4 also shows ratios of the algorithm's quiet sun spectrum with other reported reference spectra.

Constant bolometric and wavelength-dependent coefficients, shown in Figure 5, linearly scale the facular brightening and sunspot darkening inputs to produce corresponding irradiance increments that are then applied to adjust the baseline irradiance, either increasing or decreasing it depending on the wavelength-dependent strengths of the facular and sunspot influences at that time. The bolometric and wavelength-dependent coefficients are included as part of the algorithm. Additional (invariant) data also specified in the algorithm are the angles of the solar rotation axis and the ecliptic plane, termed the beta angle, throughout the year. This angle is used to adjust the projection of sunspot areas to the direction of the Earth, as it orbits the Sun.

New versions of the model are generated when and if the coefficients are determined to need revision, based on additional observations and analysis sufficient to permit reformation of the model coefficients.

### 3.3.3 Derived Data

Once the facular brightening and sunspot blocking inputs are obtained, they are linearly scaled to convert them to equivalent increments of total and spectral irradiance, which are then added to the baseline (quiet) total and spectral irradiance to determine solar irradiance at time  $t$  as specified in Section 3.2. The application of the irradiance increments to the baseline spectral irradiance is implemented in 1 nm bins on 0.5 nm grid centers. The 1 nm spectral irradiance thus calculated is then averaged into 3785 wavelength bins of varying width:

1 nm bins on wavelengths grid centers from 115.5 to 749.5 nm	(635 bins)
5 nm bins on wavelength grid centers from 752.5 to 4997.5 nm	(850 bins)
10 nm bins on wavelength grid centers from 5005.0 to 9995.0 nm	(500 bins)
50 nm bins on wavelength grid centers from 10025.0 to 99975.0 nm	(1800 bins)

There are no further processing steps; the calculated total and spectral irradiance are then written to output files. A time series of the output total solar irradiance since 1978 is shown in Figure 6 and examples of the corresponding solar spectral irradiance outputs binned in broad wavelength bands are shown in Figure 7.

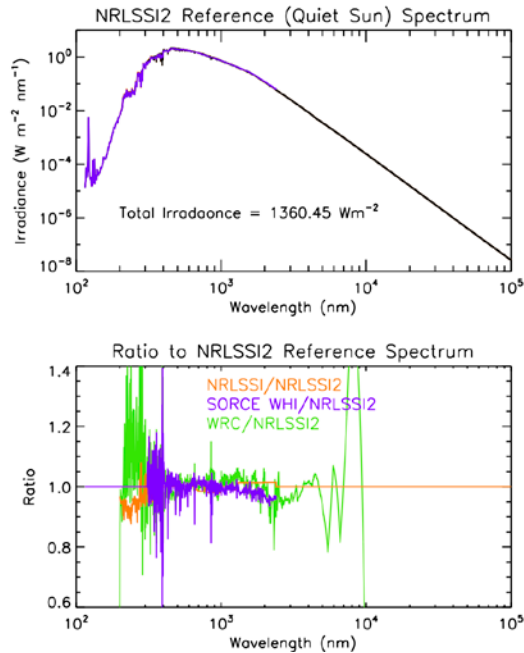


**Figure 4.** Reference spectrum of the quiet sun adopted for the NRLSSI2 irradiance variability model used in the algorithm (upper) and comparisons with other spectra (lower).

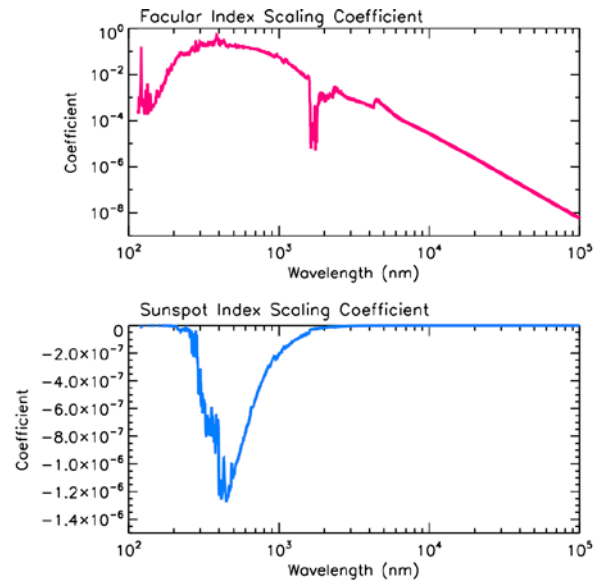


**Figure 5.** Scaling coefficients that the algorithm uses to convert the facular brightening and sunspot darkening indices in Figures 2 and 3 to their equivalent irradiance change, in energy units.

Because validation of the facular brightening and sunspot darkening inputs is crucial for reliable solar irradiance calculations, the processed facular brightening and sunspot darkening time series (e.g., Figure 2) used in the algorithm are output to a separate file, to facilitate validation with independent datasets.

### 3.3.4 Forward Models

Not applicable.

## 3.4 Theoretical Description

The overall approach of the Solar Irradiance Climate Data record algorithm builds on, and advances, the NRLTSI and NRLSSI models, as described in Lean (2000), Lean et al. (2005) and summarized in Lean and Woods (2010). Developed over a decade ago, prior to the launch of the Solar Radiation and Climate Experiment (SORCE) spacecraft (Rottman et al., 2005), the NRLTSI and NRLSSI solar irradiance variability models have been widely used for a variety of model simulations of climate and atmospheric change, including for the IPCC reports (e.g., Schmidt et al., 2011), and compared as well with other solar spectral irradiance variability models (Thuiller et al., 2013).

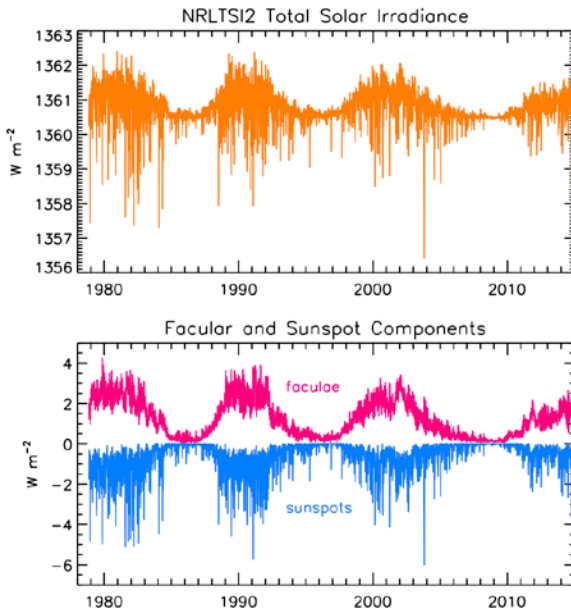


**Figure 6. Total solar irradiance reconstructed with the NRLTSI2 model algorithm (upper), and the corresponding individual facular and sunspot contributions to the total solar irradiance variations (lower).**

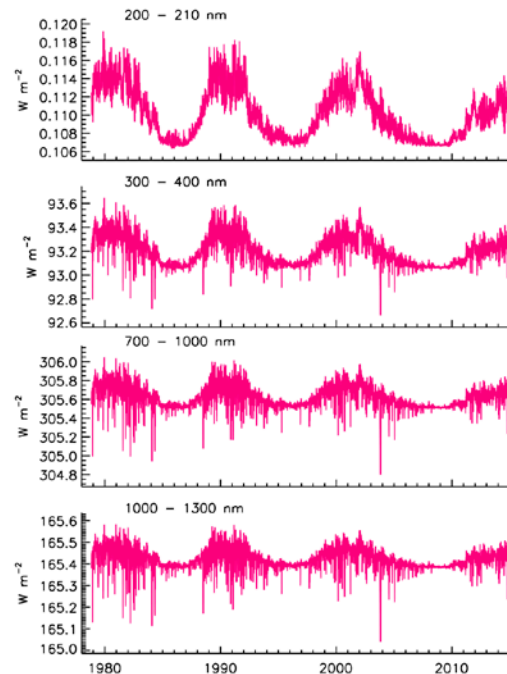


**Figure 7. Solar spectral irradiance variations calculated by the NRLSSI2 model algorithm during recent solar cycles and binned in four broad wavelength bands.**

### ***Original NRLTSI and NRLSSI Models***

The NRLTSI model was formulated using a composite of total solar irradiance constructed by Fröhlich and Lean (2004), by combining observations made by Nimbus 7, ACRIM on SMM and UARS and PMOD on SOHO. The NRLSSI model was constructed for wavelengths less than 400 nm from a linear association of spectral irradiance variations observed by the Solar Stellar Irradiance Comparison Experiment (SOLSTICE, Rottman, 2000), relative to a reference spectrum (the average SOLSTICE spectrum during the UARS time period), with corresponding changes in facular brightening and sunspot darkening, also relative to their respective reference values (Lean et al., 1997).

Lacking observations of solar spectral irradiance variability at wavelengths longer than  $\sim 400$  nm, NRLSSI's spectral irradiance variations in the visible and infrared spectral regions were determined from the wavelength-dependence of the sunspot and facular contributions, according to their respective theoretical contrasts (ratio of emission to the background quiet solar atmosphere) determined in a theoretical solar atmosphere model (Unruh et al., 2000). For the quiet irradiance spectrum a composite was compiled on a 1 nm grid from space-based observations made by SOLSTICE on UARS (from 120 to 401 nm) and SOLSPEC on the ATLAS shuttle mission (from 401 to 874 nm, Thuillier et al., 1998), and a theoretical spectrum at longer wavelengths (Kurucz, 1991). The agreement among these three spectra in their regions of overlap is better than 2%, which is well within their absolute measurements uncertainties

(Thuillier et al., 1998). The initially compiled composite spectrum was multiplied by 0.99 at all wavelengths to make its integral equal the independently measured total irradiance of the quiet Sun, whose most likely value at that time was considered to be  $1365.5 \text{ Wm}^{-2}$ .

Neither Lean (2000) nor Lean et al (2005) refer explicitly to the spectral irradiance calculations, described above, as the NRLSSI model. Following the extension of the model to include the extreme ultraviolet spectrum (Lean et al., 2011), the designation NRLSSI was chosen (e.g., as summarized in Lean and Woods, 2010) to collectively describe an empirical capability to specify the entire solar spectral irradiance and its variability from 1 to 100,000 nm. The NRLSSI model calculates the solar spectral irradiance in 1 nm bins across the entire electromagnetic spectrum, daily since 1882, monthly since 1882 and annually since 1610.

### ***Newly Formulated NRLTSI2 and NRLSSI2 Models***

The measurements made by the Total Irradiance Monitor (TIM), Solar Irradiance Monitor (SIM) and SOLSTICE instruments on the SORCE spacecraft have provided new observations of total and spectral irradiance variability throughout the descending phase of solar cycle 23 and the ascending phase of cycle 24. New versions of irradiance variability models, designated NRLTSI2 and NRLSSI2, have been formulated directly from the TIM and SOLSTICE/SIM observations, and are implemented in the Solar Irradiance Data record algorithm that this C-ATBD describes.

TIM's measurements indicate that the actual total irradiance of the quiet sun is  $\sim 5 \text{ Wm}^{-2}$  lower than in NRLTSI (Kopp and Lean, 2011), and the NRLTSI2 and NRLSSI2 models are consistent with this new, lower value of total solar irradiance.

As described in Section 3.2, the basic formulation of time-dependent total and spectral solar irradiance,  $T(t)$  and  $I(\lambda, t)$ , determines their variations arising from faculae and sunspots superimposed on specified, invariant, quiet sun reference values,  $T_Q(t)$  and  $I_Q(\lambda, t)$  (Figure 4), as,

$$T(t) = T_Q + \Delta T_F(t) + \Delta T_S(t)$$

$$I(\lambda, t) = I_Q(\lambda) + \Delta I_F(\lambda, t) + \Delta I_S(\lambda, t)$$

where  $\Delta T_F(t)$  and  $\Delta I_F(\lambda, t)$  are functions of the facular brightening index,  $F(t)$ , and  $\Delta T_S(t)$  and  $\Delta I_S(\lambda, t)$  are functions of the sunspot darkening index,  $S(t)$ . Specifically, for the NRLTSI2 total irradiance variability model

$$\Delta T_F(t) = a_F + b_F \times [F(t) - F_Q]$$

$$\Delta T_S(t) = a_S + b_S \times [S(t) - S_Q]$$

where  $F_Q$  and  $S_Q (= 0)$  are the values of the facular brightening and sunspot darkening indices corresponding to  $T_Q$ , i.e., for the quiet sun. The  $F(t)$  and  $S(t)$  are calculated using independent solar observations made approximately daily, respectively, the Mg index of global (i.e., disk integrated) facular emission and information about the area and locations of sunspot active regions on the solar disk, as described in Section 3.3.1.

The corresponding facular brightening and sunspot darkening components in the NRLSSI2 spectral irradiance variability model are

$$\Delta I_F(\lambda, t) = c_F(\lambda) + d_F(\lambda) \times [F(t) - F_Q + \Delta F(t)]$$

$$\Delta I_S(\lambda, t) = c_S(\lambda) + d_S(\lambda) \times [S(t) - S_Q + \Delta S(t)]$$

The  $a$ ,  $b$ ,  $c(\lambda)$  and  $d(\lambda)$  coefficients for faculae and sunspots are specified (Figure 5) and supplied with the algorithm. Note that the  $a$  and  $c$  coefficients are nominally zero so that when  $F=F_Q$  and  $S=S_Q$  then  $T=T_Q$  and  $I=I_Q$ . The additional facular and sunspot index increments,  $\Delta F(t)$  and  $\Delta S(t)$ , are included in the model formulation to provide small adjustments to ensure that numerically

$$T(t) = \int_{\lambda_0}^{\lambda_\infty} I(\lambda, t) d\lambda$$

$$\Delta T_F(t) = \int_{\lambda_0}^{\lambda_\infty} \Delta I_F(\lambda, t) d\lambda$$

$$\Delta T_S(t) = \int_{\lambda_0}^{\lambda_\infty} \Delta I_S(\lambda, t) d\lambda$$

Ideally, were the  $F(t)$  and  $S(t)$  physically and observationally “perfect” indicators of the sunspot and faculae sources at each wavelength, then the index increments  $\Delta F(t)$  and  $\Delta S(t)$  would be zero. Improvements in  $F(t)$  and  $S(t)$  may enable this in future versions of the algorithm.

The NRLTSI2 model uses multiple linear regression to determine the scaling coefficients of the facular brightening and sunspot darkening time series that best reproduce the total solar irradiance variability measure directly by TIM from 2003 to 2014:

$$T_{mod}(t) - T_Q = a + b_F \times [F(t) - F_Q] + b_S \times [S(t) - S_Q]$$

The observed,  $T_{TIM}$  and modeled,  $T_{mod}$ , total solar irradiance have a correlation coefficient of 0.96 and the standard deviation of the residuals,  $T_{TIM} - T_{mod}$ , is  $0.1 \text{ Wm}^{-2}$ .

Because SIM’s calibration is significantly less stable than is TIM’s, it is likely that instrumental trends are present in SIM’s solar spectral irradiance measurements (Lean and DeLand, 2012). This precludes the formulation of reliable models of solar spectral irradiance from the SIM observations, directly, as is implemented to formulate  $T_{mod}(t)$  from TIM observations. Instead, a relationship of solar spectral irradiance variability to sunspot darkening and facular brightening is first determined using observations of solar rotational modulation: instrumental trends are smaller over the (much) shorter rotational times scales than during the solar cycle. For each 1 nm bin, the observed (by SOLSTICE and SIM on SORCE) solar spectral irradiance and the facular brightening and sunspot darkening indices are detrended by subtracting 81-day running means. Multiple linear regression is then used to determine the relationships of the detrended time series:

$$\begin{aligned}
 I_{mod}^{detrend}(\lambda, t) &= I_{mod}(\lambda, t) - I_{smooth}(\lambda, t) \\
 &= c(\lambda) + d_F^{detrend}(\lambda) \times [F(t) - F_{smooth}(t)] + d_S^{detrend}(\lambda) \\
 &\quad \times [S(t) - S_{smooth}(t)]
 \end{aligned}$$

The range of facular variability in the detrended time series is smaller than during the solar cycle which, together with the “imperfect” natures of the facular brightening (and sunspot darkening) indices, causes the coefficients of models developed from detrended time series to differ from those developed from direct (i.e., not detrended) observations.

The total solar irradiance observations are used to numerically determine ratios of the coefficients obtained from multiple regression using direct observations of solar irradiance with those obtained from multiple regression of detrended observations. A second model of the TIM observations was formulated analogous to that used for NRLTSI2, but using detrended, instead of direct, time series. The ratios of the coefficients for the two different approaches are then used to adjust the coefficients for spectral irradiance variations at wavelength longer than 295 nm (where faculae and sunspots both modulate solar spectral irradiance), determined from the detrended time series. At these wavelength,  $d_S$  and  $d_F$  are estimated as

$$\begin{aligned}
 d_F &= d_F^{detrend} \left( \frac{b_F}{b_F^{detrend}} \right) \\
 d_S &= d_S^{detrend} \left( \frac{b_S}{b_F^{detrend}} \right)
 \end{aligned}$$

For wavelengths shorter than 290 nm where faculae are the dominant cause of irradiance variability (and  $d_S(\lambda) \sim 0$ ), the adjustments for the coefficients were estimated using the Call K time series, a facular index that is independent of the Mg II index, and a well-recognized indicator of UV spectral irradiance variability.

The value of  $\Delta F(t)$  is determined empirically by comparing the residual,  $R_{fac}(t)$ , of the integrated spectral irradiance facular brightening, evaluated initially with  $\Delta F(t)=0$ , with the total solar irradiance facular brightening i.e.,

$$R_{fac}(t) = a + b_F \times [F(t) - F_Q] - \sum (c_F(\lambda) + d_F(\lambda) \times [F(t) - F_Q])$$

then linearly relating this residual energy to the facular brightening index

$$R_{fac} = e_F \times [F(t) - F_Q]$$

from which the equivalent increment in the facular brightening index is determined as

$$\Delta F(t) = \frac{R_{fac}(t)}{b_F} = \frac{e_F \times [F(t) - F_Q]}{b_F}$$

Similarly,  $\Delta S(t)$  is determined empirically by comparing the residual,  $R_{spot}(t)$ , of the integrated spectral irradiance sunspot darkening evaluated initially with  $\Delta S(t)=0$ , with the total solar irradiance sunspot darkening i.e.,

$$R_{spot}(t) = b_S \times [S(t) - S_Q] - \sum (c_S(\lambda) + d_S(\lambda) \times [S(t) - S_Q])$$

then linearly relating this residual energy to the sunspot darkening index

$$R_{spot} = e_S \times [S(t) - S_Q]$$

from which the equivalent increment in the sunspot darkening index is determined as

$$\Delta S(t) = \frac{R_{spot}(t)}{b_S} = \frac{e_S \times [S(t) - S_Q]}{b_S}$$

The average difference between the spectrally integrated NRLSSI2 model and the NRLTS12 model from 1978 to 2014 is  $0.015 \text{ W m}^{-2}$  and the standard deviation of the differences is  $0.004 \text{ W m}^{-2}$ .

### ***Speculated Irradiance Changes beyond the Solar Cycle***

As well as being a dominant determinant of solar cycle irradiance variations, faculae are speculated to cause longer-term (decadal to centennial) irradiance changes. Specifying the past evolution of the facular signal is therefore necessary for reconstructing historical irradiance variations. But unlike the sunspot signal, which is suggested by direct observations of sunspot numbers since (at least) 1610, the facular component is highly uncertain and dependent essentially on somewhat ambiguous circumstantial evidence. For example, based on current observations of facular contrast and disk coverage, the disappearance of all faculae from the Sun's surface is estimated to decrease total solar irradiance about 0.1% (Lean et al., 1992). Attempts have been made to translate variations in the chromospheric activity in Sun-like stars to a plausible range of the facular influence on solar irradiance (Lean et al., 1992, 1995), with results broadly consistent with inferences from the cosmogenic and geomagnetic indices. Changes in solar structure are also considered as possible sources of long-term irradiance variations in addition to, or instead of, facular variations (Hoyt and Schatten, 1993; Tapping et al., 2007) producing levels as much as 0.3% below contemporary solar minima values (e.g., review of Maunder Minimum levels in Lean et al., 2005).

In the original version of NRLSSI (Lean, 2000) the long-term "background" component of the facular index,  $F_{BG}(t)$ , was specified as a 15-year running mean of annual sunspot group numbers in which the reduction from the quiet Sun to the Maunder Minimum is 92% of the increase in  $F_{BG}(t)$  from the quiet Sun to cycle maximum (monthly average for November 1989). These changes mimicked the reduced Ca fluxes in non-cycling Sun-like stars compared with the range of fluxes in cycling Sun-like stars (Radick et al., 1998 and Lean et al., 2001, provide additional details) which at the time of the NRLSSI model formulation were thought to exemplify long-term solar irradiance changes. However, a subsequent reassessment of the stellar data was unable to recover the original bimodal separation of (lower) Ca emission in non-cycling stars

(assumed to be in Maunder Minimum type states) compared with (higher) emission in cycling stars (Hall and Lockwood, 2004). Nor do long-term trends in the aa index and cosmogenic isotopes (generated by open flux) necessarily imply equivalent long-term trends in solar irradiance (which track closed flux) according to simulations of the transport of magnetic flux on the Sun and propagation of open flux into the heliosphere (Lean et al., 2002; Wang et al., 2005).

These developments motivated revision of the long-term “background” component of the NRLSSI model using a flux transport model to estimate the plausible magnitude of a long-term secular facular component. The flux transport model (with variable meridional flow) simulates the eruption, transport, and accumulation of magnetic flux on the Sun’s surface from the Maunder Minimum to the present in strengths and numbers proportional to the sunspot number (Wang et al., 2005). The model estimated variations in both open and total flux arising from the deposition of bipolar magnetic regions (active regions) and smaller-scale ephemeral regions on the Sun’s surface: The open flux compares reasonably well with the geomagnetic and cosmogenic isotopes, which gives confidence that the approach is plausible. A small accumulation of total flux (and possibly ephemeral regions) produces a net increase in facular brightness that, in combination with sunspot blocking, permits the reconstruction of total solar irradiance.

The increase in total solar irradiance from the Maunder Minimum to the present-day quiet Sun is about 0.04%, based on the flux transport model simulations. For comparison, because of the larger background facular component adopted in Lean (2000), the increase from the Maunder Minimum to the present-day quiet Sun in the original version of the NRLSSI model is about 0.16%, four times larger. (See Lean et al., 2005, for comparison of different estimates of TSI from the Maunder minimum to the present). The spectral irradiance changes in the NRLSSI2 model are consistent with the Wang et al. (2005) flux transport simulations and were obtained by using a background component 27% of that adopted in the spectral irradiance reconstructions of Lean (2000).

### 3.4.1 Physical and Mathematical Description

The NRLTSI2 and NRLSSI2 models, which the Solar Irradiance Climate Data record algorithm utilizes, assume that bright faculae and dark sunspots are the only causes of solar irradiance variability on contemporary time scales. The occurrence of these features on the Sun varies during the Sun’s 11-year activity cycle, producing a prominent 11-year cycle in solar irradiance. The rotation of the Sun on its axis alters the population of faculae and sunspots projected to earth, producing an additional 27-day irradiance modulation.

Following the approach of Lean et al. (1998), when the sun is inactive, the “quiet” irradiance at the Earth (at a distance of 215 times the solar radius) is determined by integrating the radiance,  $R(\lambda, 1)$ , at the center of the disk ( $\mu = 1$ ) over the entire disk using the center-to-limb function,  $L(\lambda, \mu)$  to define the ratio of  $R(\lambda, \mu)$  to  $R(\lambda, 1)$  at heliocentric position  $\mu$ , which ranges from 0 (at the disk’s limb) to 1 (at disk center). Thus the irradiance of the quiet sun is

$$I_Q(\lambda) = \frac{2\pi R_Q(\lambda, 1) \int_0^1 L(\lambda, \mu) \mu d\mu}{(215)^2}$$

$$T_Q = \int_{\lambda_0}^{\lambda_\infty} I_Q(\lambda) d\lambda$$

Magnetic features – dark sunspots and bright faculae – when present on the solar disk solar disk alter the otherwise homogeneous distribution of radiance, and hence the irradiance at the Earth, which is at some (non-quiet) time,  $t$ , given as

$$I(\lambda, t) = \frac{2\pi R_Q(\lambda, 1) \int_0^1 C(\lambda, \mu) L(\lambda, \mu) \mu d\mu}{(215)^2}$$

where

$$C(\lambda, \mu) = \frac{R(\lambda, \mu)}{R_Q(\lambda, \mu)}$$

is the ratio of the Sun's radiance at heliocentric location,  $\mu$ , relative to the radiance of the surrounding quiet Sun. This ratio is termed the contrast.

Separating radiance elements on the solar disk into those that are brighter than, darker than or equal to the quiet sun radiance permits expression of the irradiance as

$$I(\lambda, t) = I_Q(\lambda) + \frac{2\pi R_Q(\lambda, 1)}{(215)^2} \int_0^1 [C_F(\lambda, \mu) - 1] L(\lambda, \mu) \mu d\mu \\ + \frac{2\pi R_Q(\lambda, 1)}{(215)^2} \int_0^1 [C_S(\lambda, \mu) - 1] L(\lambda, \mu) \mu d\mu$$

where  $C_F(\lambda, \mu)$  and  $C_S(\lambda, \mu)$  are the contrasts of the faculae and sunspots, respectively. For the number of radiance elements defined as faculae,  $N_{fac}$ , and sunspots,  $N_{spot}$ , with actual area on the solar surface of  $A_{fac}$  and  $A_{spot}$ , at a given time,  $t$ , the corresponding solar irradiance is (with  $A = 2\pi r_{sun}^2 d\mu$  for solar radius  $r_{sun}$ )

$$I(\lambda, t) = I_Q(\lambda) + \frac{2\pi R_Q(\lambda, 1)}{(215)^2} \sum_1^{N_{fac}} [C_F(\lambda, \mu) - 1] L(\lambda, \mu) \mu \frac{A_{fac}}{2\pi r_{sun}^2} \\ + \frac{2\pi R_Q(\lambda, 1)}{(215)^2} \sum_1^{N_{spot}} [C_S(\lambda, \mu) - 1] L(\lambda, \mu) \mu \frac{A_{spot}}{2\pi r_{sun}^2}$$

which is analogous to the basic formulation used in the Solar Irradiance Climate Data Record algorithm for the solar spectral irradiance:

$$I(\lambda, t) = I_Q(\lambda) + \Delta I_F(\lambda, t) + \Delta I_S(\lambda, t)$$

where

$$\Delta I_F(\lambda, t) = \frac{2\pi R_Q(\lambda, 1)}{(215)^2} \sum_1^{N_{fac}} [C_F(\lambda, \mu) - 1] L(\lambda, \mu) \mu \frac{A_{fac}}{2\pi r_{sun}^2}$$

$$\Delta I_S(\lambda, t) = \frac{2\pi R_Q(\lambda, 1)}{(215)^2} \sum_1^{N_{spot}} [C_S(\lambda, \mu) - 1] L(\lambda, \mu) \mu \frac{A_{spot}}{2\pi r_{sun}^2}$$

The corresponding total solar irradiance is

$$T(t) = \int_{\lambda_0}^{\lambda_\infty} I_Q(\lambda) d\lambda$$

$$T(t) = \int_{\lambda_0}^{\lambda_\infty} I_Q(\lambda) d\lambda + \int_{\lambda_0}^{\lambda_\infty} \Delta I_F(\lambda, t) d\lambda + \int_{\lambda_0}^{\lambda_\infty} \Delta I_S(\lambda, t) d\lambda$$

which is analogous to the basic formulation used in the Solar Irradiance Climate Data Record algorithm for the total spectral irradiance:

$$T(t) = T_Q + \Delta T_F(t) + \Delta T_S(t)$$

$$\frac{\Delta T(t)}{T_Q} = 1 + \frac{\Delta T_F(t)}{T_Q} + \frac{\Delta T_S(t)}{T_Q}$$

The calculation of the sunspot darkening index in Section 3.3.1 is physically an estimate of  $\frac{\Delta T_S}{T_Q}$  made using the above theoretical basis with a number of assumptions and parameterizations, as follows. The center-to-limb variation is assumed to be independent of wavelength and specified as

$$L(\mu) = \frac{3\mu + 2}{5}$$

$$\int_0^1 L(\mu) d\mu = \int_0^1 \frac{3\mu + 2}{5} \mu d\mu = \frac{2}{5}$$

The sunspot contrast  $C_S(\lambda) = R_S(\lambda) / R_Q(\lambda)$  is assumed to be independent of  $\mu$  and its bolometric (i.e., spectrally integrated) value nominally 0.32. The sunspot area,  $A_S$ , that NOAA reports is in millionths of the solar hemisphere, i.e.,

$$A_S = \frac{A_{spot}}{2\pi r_{sun}^2} \times 10^6$$

Typically, information about sunspot areas and locations are recorded at different times throughout the day (depending on local time) by a dozen or so different ground-based stations. The sunspot darkening index used to evaluate NRLTSI2 and NRLSSI2, shown in Figure 6, is the average of all the available information on a given day. As well, individual sites calculate

sunspot darkening factors, and it has also been applied to space-based white light images made by MDI on SOHO (F. Watson, <http://www.nso.edu/staff/fwatson/STARA>).

With the above assumptions,

$$\begin{aligned}
 \frac{\Delta T_S(t)}{T_Q} &= \frac{\int_0^\infty \frac{2\pi R_Q(\lambda, 1)}{(215)^2} \sum_1^{N_{spot}} A_S [C_S(\lambda) - 1] L(\mu) \mu d\lambda}{\int_0^\infty \frac{2\pi R_Q(\lambda, 1)}{(215)^2} \int_0^1 L(\mu) \mu d\lambda} \\
 &= \sum_n^{N_{spot}} A_S \frac{(3\mu + 2)}{5} \mu \frac{\int_0^\infty R_Q(\lambda, 1) [C_S(\lambda) - 1] d\lambda}{\int_0^\infty R_Q(\lambda, 1) d\lambda} \times \frac{5}{2} \\
 &= \sum_n^{N_{spot}} A_S \frac{(3\mu + 2)}{2} \mu \frac{\int_0^\infty R_Q(\lambda, 1) [C_S(\lambda) - 1] d\lambda}{\int_0^\infty R_Q(\lambda, 1) d\lambda} \\
 &= \sum_n^{N_{spot}} A_S \frac{(3\mu + 2)}{2} \mu (C_S^B - 1)
 \end{aligned}$$

The facular brightening can be calculated similarly to the sunspot darkening index, which Lean et al. (1998) demonstrate for the irradiance at 200 nm using histograms of calibrated Ca K solar images to identify bright faculae. However, for practical applications, the characteristics of facular are in general poorly observed in solar imagery and inadequately specified compared with the more compact, darker and relatively well-defined sunspot regions. Furthermore, whereas sunspot regions are typically discrete and therefore relatively easily quantified, faculae occur with a continuous distribution of sizes and contrasts, so that statistical definitions (which can be ambiguous) are needed for practical quantification. Because of the lack of reliable quantitative data for facular areas, center-to-limb functions and contrasts, the NRLSSI2 model (like NRLSSI) calculates spectral irradiance change due to faculae as a linear function of a “flux” (i.e., disk-integrated) proxy of facular brightening,  $F(t)$ .

### 3.4.2 Data Merging Strategy

No data merging is needed for the NRLTSI2 and NRLSSI2 models to calculate solar irradiance.

### 3.4.3 Numerical Strategy

The NRLTSI2 and NRLSSI2 models do not include numerical algorithms.

### 3.4.4 Calculations

The algorithm calculates the total and solar spectral irradiance using an IDL procedure to applying the previously derived (and constant in time) coefficients to scale the two inputs, the facular brightening and sunspot darkening indices.

### 3.4.5 Look-Up Table Description

There are no designated Look-Up tables, per se, that the algorithm needs to repeatedly accesses. The algorithm does require as initial input the spectral irradiance of the quiet sun, specified in 1 nm bins from 115.5 to 999,999.5 nm, as well as the coefficients (on the same 1 nm wavelength grid) to convert the input facular brightening and sunspot darkening indices to irradiance changes at any given time. These constant values are considered to be part of the overall algorithm, but could also be separately formulated and reconsidered as Look Up Tables.

### 3.4.6 Parameterization

There are no parameterizations aside from the conversion of the facular brightening and sunspot darkening indices to irradiance units, using the specified coefficients.

### 3.4.7 Algorithm Output

#### *Total Solar Irradiance (TSI)*

The NRLTSI2 model produces a value and associated uncertainty of total solar irradiance on an absolute scale defined by the measurements made by TIM on SORCE, for given inputs of the facular brightening and sunspot darkening indices, estimated daily using inputs from ground and space-based solar observations when available, as specified above.

Typical total solar irradiance output files in NetCDF4 format have the structure identified in Table 3. The files follow CF-1.6 metadata conventions for variable names and attributes.

**Table 3. Structure of the algorithm (NRLTSI2) output of Total Solar Irradiance (TSI).**

Variable Name	Long Name	Standard Name	Units	Missing Value
TSI	NOAA Climate Data Record of Daily Total Solar Irradiance (W m <sup>-2</sup> )	solar_irradiance	W m <sup>-2</sup>	-99.0
TSI_UNC	Uncertainty in daily total solar irradiance		W m <sup>-2</sup>	-99.0
time		time	days since 1610-01-01 00:00:00.0	-99.0
time_bnds	Minimum (inclusive) and maximum (exclusive) dates included in the time averaging		days since 1610-01-01 00:00:00.0	

The TSI values are aggregated in several time averaging formats to support the projected needs of the user communities. The initial transition of the Solar Irradiance Climate Data Record to NOAA includes separate, daily and monthly-averaged modeled TSI values from 1882 through 2014, aggregated into yearly files. Additionally provided are annually-averaged TSI from 1610 through 2014, aggregated into a single, period of record, file. Preliminary, quarterly updates in the daily and monthly-averaged TSI will be produced operationally. At each subsequent year-end, the preliminary files will be replaced by final values of daily and monthly-averaged TSI,

aggregated into a year-long record. Yearly updates to the annually-averaged TSI will be incorporated into a new, period of record file.

The time averaging in the data will be identified using the *time\_bounds* variable in the netCDF4 output.

The file naming conventions for the TSI data described above is as follows:

**<product>\_<version>\_<type>\_s<YYYYmmdd>\_e<YYYYmmdd>\_c<YYYYmmdd>.nc**

where,

<product> is 'tsi' for total solar irradiance,

<version> is the product version number (for the initial release, this is v02r00 for final data, and v02r00-preliminary for preliminary version data),

<type> is type of time average ('daily' for daily data, 'monthly' for monthly averaged data, and 'yearly' for annually averaged data)

s<YYYYMMDD> is the start year, month, and day of the data in the file,

e<YYYYMMDD> is the end year, month, and day of the data in the file, and

c<YYYYMMDD> is the creation of processing data of the file.

A file name example is tsi\_v02r00\_daily\_s20010101\_e20011231\_c20150131.nc.

The start, s<>, and end, e<>, formats vary based on whether the irradiance values are daily, monthly or annually averaged. For example, the time format for daily TSI values follows YYYYMMDD convention, monthly-averaged TSI values follows YYYYMM convention, and annually-averaged TSI values follows YYYY convention.

### ***Solar Spectral Irradiance (SSI)***

The NRLSSI2 model produces solar spectral irradiance values, and associated uncertainties, on an absolute scale such that the integrated spectral irradiance is equivalent to the total irradiance observed by TIM on SORCE, for given inputs of the facular brightening and sunspot darkening indices, estimated daily using data from ground and space-based solar observations when available, as specified above.

Typical solar spectral irradiance output files in NetCDF4 format have the structure identified in Table 4. The files follow CF-1.6 metadata conventions for variable names and attributes. Due to file size consideration, the uncertainties in SSI are not written to output. Table 6 provides representative SSI values and uncertainties. The science product for solar spectral irradiance also contains the value of TSI, and its associated uncertainty, because users interested in SSI (for example, climate modelers) also require the integrated quantity to constrain the total incoming solar irradiance. By including the TSI with the SSI science product, we provide the user community the necessary values in a single file.

The initial transition of the Solar Irradiance Climate Data Record to NOAA includes separate, daily and monthly-averaged modeled SSI values from 1882 through 2014, aggregated into yearly files. Additionally provided are annually-averaged SSI from 1610 through 2014, aggregated into a single, period of record, file. Preliminary, quarterly updates in the daily and

monthly-averaged SSI will be produced operationally. At each subsequent year-end, the preliminary files will be replaced by final values of daily and monthly-averaged SSI, aggregated into a year-long record. Yearly updates to the annually-averaged SSI will be incorporated into a new, period of record file.

The time averaging in the data will be identified using the *time\_bounds* variable in the netCDF4 output.

The file naming conventions for the TSI data described above is as follows:

**<product>\_<version>\_<type>\_s<YYYYmmdd>\_e<YYYYmmdd>\_c<YYYYmmdd>.nc**

where,

<product> is 'ssi' for solar spectral irradiance,

<version> is the product version number (for the initial release, this is v02r00 for final data, and v02r00-preliminary for preliminary version data),

<type> is type of time average ('daily' for daily data, 'monthly' for monthly averaged data, and 'yearly' for annually averaged data)

s<YYYYMMDD> is the start year, month, and day of the data in the file,

e<YYYYMMDD> is the end year, month, and day of the data in the file, and

c<YYYYMMDD> is the creation of processing data of the file.

**Table 4. Structure of the algorithm (NRLSSI2) output for values of Solar Spectral Irradiance (SSI).**

Variable Name	Long Name	Standard Name	Units	Missing Value
SSI	NOAA Climate Data Record of Daily Solar Spectral Irradiance ( $\text{W m}^{-2} \text{nm}^{-1}$ )	solar_irradiance_per_unit_wavelength	$\text{W m}^{-2} \text{nm}^{-1}$	-99.0
wavelength	Wavelength grid center	radiation_wavelength	nm	N/A
Wavelength_Band_Width	Wavelength band width. Centered on wavelength.		nm	N/A
TSI	NOAA Climate Data Record of Daily Total Solar Irradiance ( $\text{W m}^{-2}$ )	toa_total_solar_irradiance	$\text{W m}^{-2}$	-99.0
TSI_UNC	Uncertainty in Daily Total Solar Irradiance ( $\text{W m}^{-2}$ )		$\text{W m}^{-2}$	-99.0
time		time	days since 1610-01-01 00:00:00.0	
time_bnds	Minimum (inclusive) and maximum (exclusive) dates included in the time averaging		days since 1610-01-01 00:00:00.0	

## 4. Test Datasets and Outputs

### 4.1 Test Input Datasets

As a first test that the algorithm is performing as expected, the total solar irradiance is compared numerically with the integral of the solar spectral irradiance, and the individual faculae and sunspot components are also compared. Figure 8 shows these comparisons. For specific versions of the solar irradiance algorithm, the comparison of NRLTSI2 and  $\Sigma$ NRLSSI2 may have slightly different offsets and standard deviations, as a result of altered facular and sunspot wavelength-dependent coefficients. The values for the mean and standard deviation of the residual time series NRLTSI2 and  $\Sigma$ NRLSSI2 given in Figure 8 corresponds to the initial version of the algorithm.

A second test for algorithm performance is comparison of selected time series of the NRLTSI2 and NRLSSI2 irradiance values that the algorithm calculates with the corresponding time series of the original NRLTSI and NRLSSI models (which have, themselves, been widely compared with available observations). Figure 9 shows such a comparison for the total solar irradiance. NRLTSI2, constructed directly from the SORCE/TIM observations, has a lower absolute scale and slightly larger variability than that of NRLTSI. Figure 10 compares the binned spectral irradiance in selected broad wavelength bands according to NRLSSI2 with the corresponding values of NRLSSI.

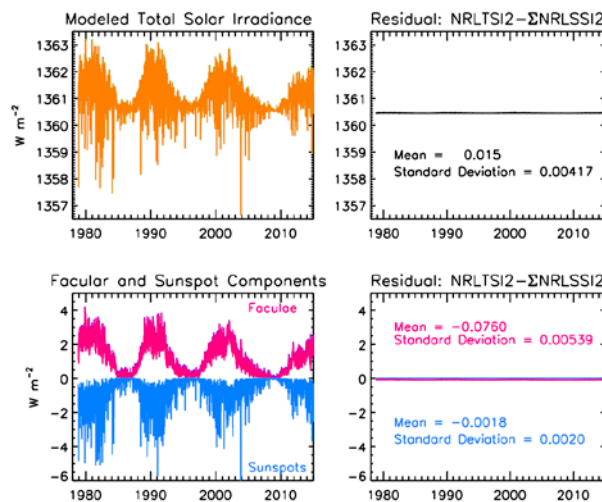


**Figure 8. Comparison of NRLTSI2 total irradiance variations calculated by the algorithm, with the integral of the NRLSSI2 spectra also calculated by the algorithm (upper), and similar comparisons of their respective facular and sunspot components (lower).**

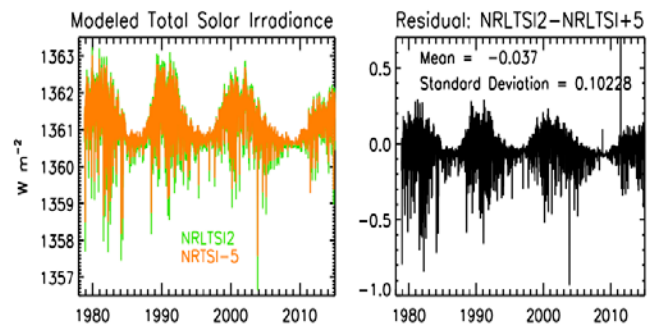


**Figure 9. Comparison of NRLTSI2 total solar irradiance variations calculated by the algorithm with an earlier model, NRLTSI.**

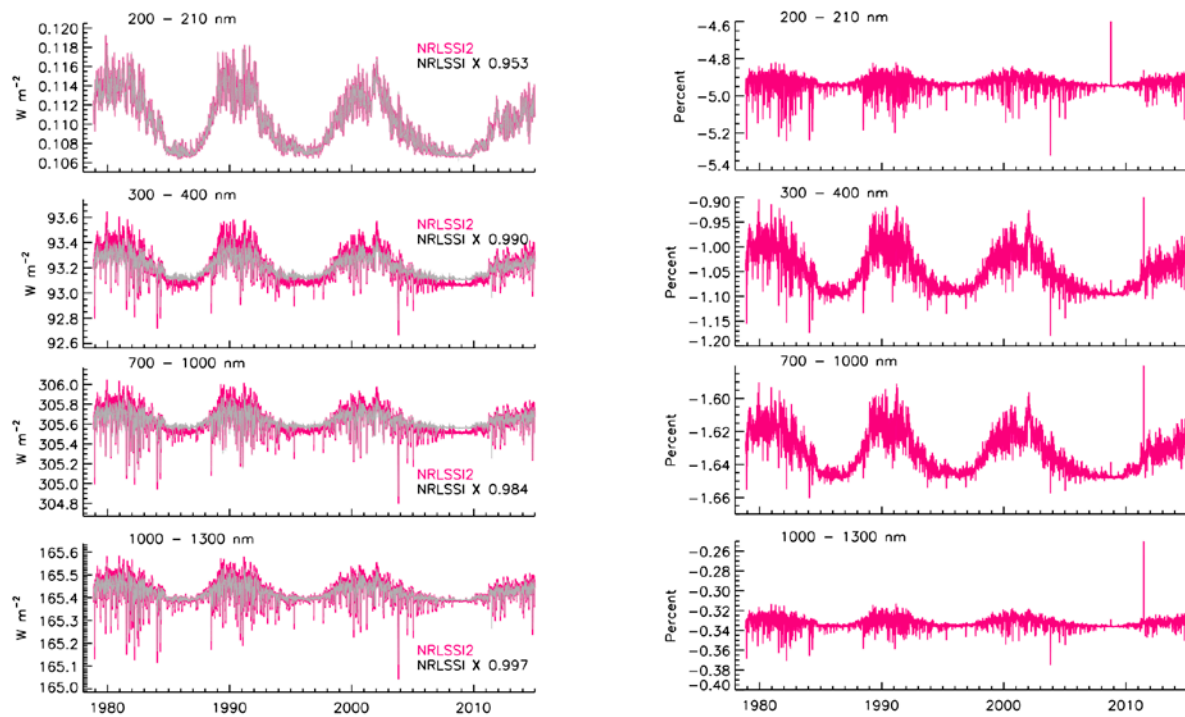


Figure 10. Comparisons of NRLSSI2 solar spectral irradiance variation calculated by the algorithm and binned in selected broad wavelength bands, as shown in Figure 7, with an earlier model, NRLSSI. On the left are the time series in energy units and on the right are percentage differences.

## 4.2 Test Output Analysis

### 4.2.1 Reproducibility

The algorithm's calculation of total and spectral irradiance is 100% numerically reproducible given identical sunspot darkening and facular brightening inputs.

### 4.2.2 Precision and Accuracy

Numerically, the algorithm itself precisely and accurately calculates the total and spectral irradiance according to the specified sunspot darkening and facular brightening inputs, the baseline (quiet) reference irradiance values and the bolometric and wavelength-dependent scaling factors. An immediate verification of the algorithm performance is the numerical comparison of the total solar irradiance,  $T(t)$ , with the integral of the solar spectral irradiance,  $\int_{\lambda_0}^{\lambda_{\infty}} I_Q(\lambda) d\lambda$ , which should agree to within a known amount, i.e.,  $T(t) \approx \int_{\lambda_0}^{\lambda_{\infty}} I(\lambda, t) d\lambda$ .

Similarly, the separate facular and sunspot components that the algorithm calculates for the total irradiance and the integrated spectral irradiance should agree to within known amounts, i.e.,  $\Delta T_F(t) \approx \int_{\lambda_0}^{\lambda_{\infty}} \Delta I_F(\lambda, t) d\lambda$  and  $\Delta T_S(t) \approx \int_{\lambda_0}^{\lambda_{\infty}} \Delta I_S(\lambda, t) d\lambda$ .

The precision and the accuracy of the derived solar irradiance depend on:

- 1) uncertainties in the absolute scale of the reference quiet sun values, which are obtained from direct solar irradiance measurements made by instruments whose calibration is traceable to National Institute of Standards and Technology (NIST) standards (Kopp and Lean, 2011).
- 2) uncertainties in the input facular brightening and sunspot darkening values, including those related to measurements of the indices (of order  $\pm 20\%$ ), and to assumptions about the indices' representations of facular brightening and sunspot darkening.
- 3) statistical uncertainties of the coefficients used to scale the facular and sunspot inputs to equivalent irradiance increments.
- 4) assumptions used to formulate the basic algorithm equations (as discussed in Section 6).

### 4.2.3 Error Budget

The original NRLTSI and NRLSSI values for modeled solar irradiance lacked accompanying error estimates. Error budgets for the total solar irradiance CDR (NRLTSI2 model) and the solar spectral irradiance CDR (NRSSI2 model) are time dependent; when the facular brightening and sunspot darkening contributions are zero (i.e., the indices achieve their minimum values,  $F(t) = F_Q$  and  $S(t) = S_Q$ ), such as may occur during solar activity minima, the error budget reduces to that of the absolute uncertainty of the adopted irradiance of the quiet sun. But when facular brightening and sunspot darkening contributions are non-zero, which is typically the case, the estimation of these additional components produces additional uncertainties that increase the error budget.

Tables 5 and 6 provide initial uncertainty estimates typical of daily total irradiance and solar spectral irradiance, respectively, during high solar activity conditions (specifically, on 30 October 2003) arising from the first three sources of uncertainty identified in Section 4.2.2. Firstly, relative uncertainties in the absolute scale of the irradiance (see second to last row in Tables 5 and 6) are conservative estimates based on those reported for the direct measurements and the differences between absolute irradiance spectra such as evident in Figure 4. Secondly, uncertainties in the change in the facular brightening and sunspot darkening indices from their minimum values, input to the algorithm, are specified as  $\pm 20\%$ ; the uncertainty in the mean sunspot darkening derived from independent stations (typically 2 to 4 per day) is of this order. Thirdly, uncertainties in the coefficients that transform the input indices to irradiance are obtained from the statistical output of the regression analyses used to construct the model that the algorithm uses. Improved estimates of uncertainties associated with the solar indices will be obtained in the future from statistical analysis of the index time series and their input data, and from comparisons with other proxies of solar indices, which are not utilized in the algorithm but can be used to monitor the accuracy and stability of the input indices.

The uncertainties written to output are those from the 2<sup>nd</sup> and 3<sup>rd</sup> sources of uncertainty listed above. Users of the solar irradiance CDR can compute the additive contribution due to the relative uncertainty in the absolute irradiance scale (the 1<sup>st</sup> source of uncertainty) in post-analysis with a user-guided value of the relative uncertainty in the absolute irradiance scale

(multiplied by the quiet sun irradiance to convert to irradiance units). For example, in Tables 5 and 6 we list the contribution to the modeled total and spectral irradiance associated with the uncertainty in the absolute irradiance scale,  $\sigma_{T_Q}$  and  $\sigma_{I_Q}(\lambda)$ .

Uncertainties arising from the assumptions used to formulate the algorithm are more difficult to assess objectively and establish quantitatively. Future work in support of ongoing efforts to produce a robust solar irradiance climate data record will extend the initial error estimates for the NRLTSI2 and NRLSSI2 modeled solar irradiance given in Tables 5 and 6, including their time and wavelength dependencies. The future uncertainty estimates will also incorporate an understanding of the impacts of the assumptions in the algorithm's theoretical basis on the derived solar irradiance (itemized in Table 7). This future understanding will reflect previous peer-reviewed studies and statistical results from the operational production of the modeled solar irradiance.

### **Total Solar Irradiance**

The total solar irradiance is determined (Section 3.4) as

$$T_{mod}(t) = T_Q + a + b_F \times [F(t) - F_Q] + b_S \times [S(t) - S_Q]$$

and the uncertainty in this determination is estimated as

$$\sigma_T(t) = \sigma_{T_Q} + \sigma_a + \sigma_{b_F \times [F(t) - F_Q]}(t) + \sigma_{b_S \times [S(t) - S_Q]}(t)$$

where

$$\left[ \frac{\sigma_{b_F \times [F(t) - F_Q]}(t)}{b_F \times [F(t) - F_Q]} \right]^2 = \left[ \frac{\sigma_{b_F}}{b_F} \right]^2 + \left[ \frac{\sigma_{F(t) - F_Q}}{[F(t) - F_Q]} \right]^2$$

and

$$\left[ \frac{\sigma_{b_S \times [S(t) - S_Q]}(t)}{b_S \times [S(t) - S_Q]} \right]^2 = \left[ \frac{\sigma_{b_S}}{b_S} \right]^2 + \left[ \frac{\sigma_{S(t) - S_Q}}{[S(t) - S_Q]} \right]^2$$

with the facular brightening  $F(t)$  specified by the University of Bremen Composite Mg II index and sunspot darkening as (Section 3.3.1)

$$S(t) = 0.32 \sum_1^{N_{spot}} A_S \left( \frac{3\mu + 2}{2} \right) \mu$$

Table 5 lists values of the quantities used to estimate the uncertainty in total solar irradiance on 30<sup>th</sup> October 2003, a day when facular brightening and sunspot darkening values were relatively high (see Figures 2 and 3). Figure 11 shows time series of total solar irradiance with time-dependent uncertainties indicated by grey shading.

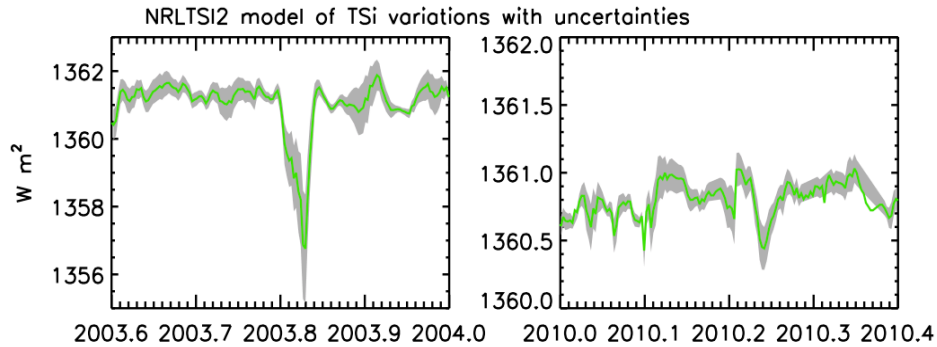


Figure 11. Examples of NRLTSI2 total solar irradiance variations and estimated uncertainties in the relative changes (i.e., excluding the  $\pm 0.5 \text{ W m}^{-2}$  uncertainty in the total solar irradiance absolute scale) that the algorithm calculates during epochs of high solar activity (left) and moderate solar activity (right).

Table 5. Representative quantities and their uncertainties, used to estimate  $1-\sigma$  relative uncertainties in the daily value of total solar irradiance produced by the algorithm on 30<sup>th</sup> October 2003, when facular brightening and sunspot darkening values were relatively high. Note that  $F_Q=0.1502$  and  $S_Q = 0$ .

Quantity	Value and Uncertainty
$a$	$0.091 \pm 0.006$
$b_F$ MgII index scalar	$139.66 \pm 1.12$
$F(t)-F_Q$ MgII index change	$0.0151 \pm 0.003$ (20%)
$b_F \times [F(t)-F_Q]$ facular TSI contribution	$2.2 \pm 0.4 \text{ W m}^{-2}$
$b_S$ sunspot index scalar	$-0.000564 \pm 0.000005$
$S(t)-S_Q$ sunspot index change	$10647 \pm 2129$ (20%)
$B_S \times [S(t)-S_Q]$ sunspot TSI contribution	$-6.0 \pm 1.2 \text{ W m}^{-2}$
$T(t) - T_Q$ TSI change from quiet sun	$-3.8 \pm (0.006 + 0.4 + 1.2) \pm 1.6$
$T_Q$	$1360.45 \pm 0.5 \text{ W m}^{-2}$
$T(t)$ absolute value	$1356.64 \pm 2.1 \text{ W m}^{-2}$

### Solar Spectral Irradiance

Solar spectral irradiance at wavelength  $\lambda$  is determined (Section 3.4) as

$$I(\lambda, t) = I_Q(\lambda) + \Delta I_F(\lambda, t) + \Delta I_S(\lambda, t)$$

where

$$\Delta I_F(\lambda, t) = c_F(\lambda) + d_F(\lambda) \times [F(t) - F_Q + \Delta F(t)]$$

$$\Delta I_S(\lambda, t) = c_S(\lambda) + d_S(\lambda) \times [S(t) - S_Q + \Delta S(t)]$$

The coefficients  $d_F$  and  $d_S$  are

$$d_F = d_F^{detrend} \left( \frac{b_F}{b_F^{detrend}} \right)$$

$$d_S = d_S^{detrend} \left( \frac{b_S}{b_S^{detrend}} \right)$$

where  $d_F^{detrend}$  and  $d_S^{detrend}$  are obtained from multiple regression of the observed, detrended solar spectral irradiance time series at wavelength  $\lambda$  (in 1 nm bins) with the detrended facular brightening and sunspot darkening indices, i.e.,

$$I_{mod}^{detrend}(\lambda, t) = c(\lambda) + d_F^{detrend}(\lambda) \times [F(t) - F_{smooth}(t)] + d_S^{detrend}(\lambda) \times [S(t) - S_{smooth}(t)]$$

and  $b_F$ ,  $b_S$  and  $b_F^{detrend}$  and  $b_S^{detrend}$  are the coefficients obtained from multiple regression of the total irradiance time series using, respectively, direct and detrended observations. Since spectral irradiance at wavelengths longer than 290 nm vary in response to both facular and sunspot influences, the total solar irradiance is an appropriate time series for estimating the ratios of the scaling coefficients when determined with and without first detrending the input irradiance and indices time series. This is not the case for spectral irradiance at wavelengths less than 290 nm, whose variations reflect primarily the facular influence. For these ultraviolet wavelengths the Call K index facular proxy measured at Sacramento Peak Observatory over multiple solar cycles is used to estimate the ratios of the scaling coefficients when determined with and without first detrending the input irradiance and indices time series.

The uncertainty in the solar spectral irradiance value is estimated as

$$\sigma_I(\lambda, t) = \sigma_{I_Q}(\lambda) + \sigma_{c_F+c_S}(\lambda) + \sigma_{d_F \times [F(t)-F_Q]}(\lambda, t) + \sigma_{d_F \times \Delta F(t)}(\lambda, t) + \sigma_{d_S \times [S(t)-S_Q]}(\lambda, t) + \sigma_{d_S \times \Delta S(t)}(\lambda, t)$$

where

$$\left[ \frac{\sigma_{d_F(\lambda)(F(t)-F_Q)}(\lambda, t)}{d_F(\lambda) \times [F(t) - F_Q]} \right]^2 = \left[ \frac{\sigma_{d_F(\lambda)}}{d_F(\lambda)} \right]^2 + \left[ \frac{\sigma_{F(t)-F_Q}}{F(t) - F_Q} \right]^2$$

$$\left[ \frac{\sigma_{d_F(\lambda)}}{d_F(\lambda)} \right]^2 = \left[ \frac{\sigma_{d_F^{detrend}(\lambda)}}{d_F^{detrend}(\lambda)} \right]^2 + \left[ \frac{\sigma_{b_F}}{b_F} \right]^2 + \left[ \frac{\sigma_{b_F^{detrend}}}{b_F^{detrend}} \right]^2$$

$$\left[ \frac{\sigma_{d(\lambda) \times \Delta F(t)}(\lambda, t)}{d_F(\lambda) \times \Delta F(t)} \right]^2 = \left[ \frac{\sigma_{d_F(\lambda)}}{d_F(\lambda)} \right]^2 + \left[ \frac{\sigma_{\Delta F(t)}}{\Delta F(t)} \right]^2$$

with facular brightening  $F(t)$  specified by the University of Bremen Composite Mg II index.

Similarly,

$$\left[ \frac{\sigma_{d_S(\lambda)(S(t)-S_Q)}(\lambda, t)}{d_S(\lambda) \times [S(t) - S_Q]} \right]^2 = \left[ \frac{\sigma_{d_S(\lambda)}}{d_S(\lambda)} \right]^2 + \left[ \frac{\sigma_{S(t)-S_Q}}{S(t) - S_Q} \right]^2$$

$$\left[ \frac{\sigma_{d_S(\lambda)}}{d_S(\lambda)} \right]^2 = \left[ \frac{\sigma_{d_S^{detrend}(\lambda)}}{d_S^{detrend}(\lambda)} \right]^2 + \left[ \frac{\sigma_{b_S}}{b_S} \right]^2 + \left[ \frac{\sigma_{b_S^{detrend}}}{b_S^{detrend}} \right]^2$$

$$\left[ \frac{\sigma_{d_S(\lambda) \times \Delta S(t)}(\lambda, t)}{d_S(\lambda) \times \Delta S(t)} \right]^2 = \left[ \frac{\sigma_{d_S(\lambda)}}{d_S(\lambda)} \right]^2 + \left[ \frac{\sigma_{\Delta S(t)}}{\Delta S(t)} \right]^2$$

with sunspot darkening as

$$S(t) = 0.32 \sum_1^{N_{spot}} A_S \left( \frac{3\mu + 2}{2} \right) \mu$$

The value of  $\Delta F(t)$  is determined empirically by comparing the residual,  $R_{fac}(t)$ , of the integrated spectral irradiance facular brightening, evaluated initially with  $\Delta F(t)=0$ , and the total solar irradiance facular brightening i.e.,

$$R_{fac}(t) = a + b_F \times [F(t) - F_Q] - \sum (c_F(\lambda) + d_F(\lambda) \times [F(t) - F_Q])$$

then linearly relating this residual energy to the facular brightening index

$$R_{fac} = e_F \times [F(t) - F_Q]$$

from which the equivalent increment in the facular brightening index is determined as

$$\Delta F(t) = \frac{R_{fac}(t)}{b_F} = \frac{e_F \times [F(t) - F_Q]}{b_F}$$

with uncertainty

$$\left[ \frac{\sigma_{\Delta F(t)}}{\Delta F(t)} \right]^2 = \left[ \frac{\sigma_{e_F}}{e_F} \right]^2 + \left[ \frac{\sigma_{b_F}}{b_F} \right]^2 + \left[ \frac{\sigma_{F(t)-F_Q}}{F(t) - F_Q} \right]^2$$

Similarly,  $\Delta S(t)$  is determined empirically by comparing the residual,  $R_{spot}(t)$ , of the integrated spectral irradiance sunspot darkening evaluated initially with  $\Delta S(t)=0$  and the total solar irradiance sunspot darkening, i.e.,

$$R_{spot}(t) = b_S \times [S(t) - S_Q] - \sum (c_S(\lambda) + d_S(\lambda) \times [S(t) - S_Q])$$

then linearly relating this residual energy to the sunspot darkening index

$$R_{spot} = e_S \times [S(t) - S_Q]$$

from which the equivalent increment in the sunspot darkening index is determined as

$$\Delta S(t) = \frac{R_{spot}(t)}{b_S} = \frac{e_S \times [S(t) - S_Q]}{b_S}$$

with uncertainty

$$\left[ \frac{\sigma_{\Delta S(t)}}{\Delta S(t)} \right]^2 = \left[ \frac{\sigma_{e_S}}{e_S} \right]^2 + \left[ \frac{\sigma_{b_S}}{b_S} \right]^2 + \left[ \frac{\sigma_{S(t)-S_Q}}{S(t) - S_Q} \right]^2$$

Shown in Figure 12 is the change in solar spectral irradiance estimated by the algorithm for 30<sup>th</sup> October 2003, a day when facular brightening and sunspot darkening values were relatively high (see Figures 2 and 3), with associated wavelength-dependent uncertainties indicated by the gray shading. This is the spectral irradiance change that accompanies the large total solar irradiance decrease seen in 2003 in Figure 11. The numerical values in Table 6 for the spectral irradiance change and uncertainties on 30 October 2003 correspond to four of the wavelengths shown in Figure 12.

The solar spectral irradiance uncertainties are time-dependent, as well as wavelength-dependent, varying as the magnitudes of the facular brightening and sunspot darkening indices wax and wane throughout the solar activity cycle. Figure 13 shows time series of the solar spectral irradiance during 2003, at the four wavelengths in Table 6; this time interval corresponds to the total irradiance and uncertainties in Figure 11.

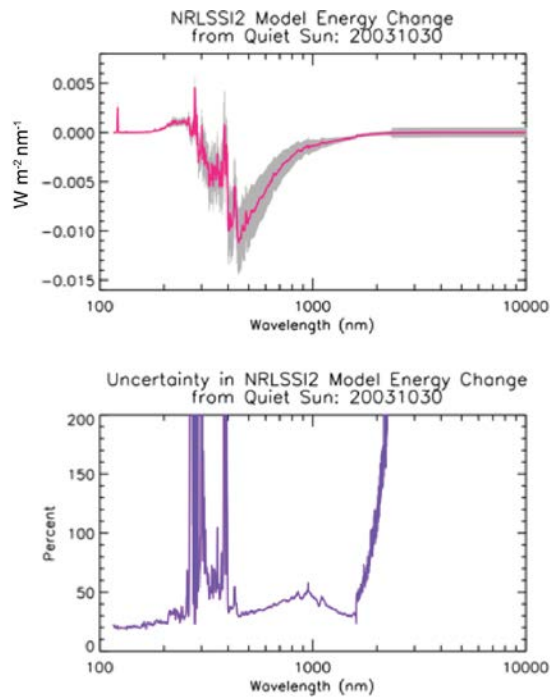


**Figure 12. Percentage uncertainties in the NRLSSI2 modeled solar spectral irradiance change typical of high solar activity, relative to the spectral irradiance of the quiet sun (i.e., excluding the uncertainty of the spectral solar irradiance absolute scale).**

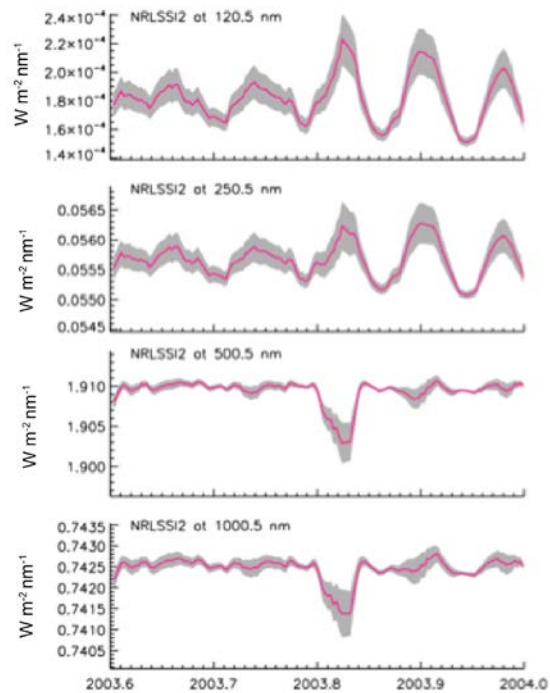


**Figure 13. Solar spectral irradiance variations calculated by the algorithm are shown for the four wavelengths listed in Table 6, with estimated uncertainties in the relative changes (i.e., excluding the uncertainty of the total solar irradiance absolute scale) during an epoch of relatively high solar activity.**

**Table 6. Representative quantities and their uncertainties, used to estimate 1- $\sigma$  uncertainties in daily values of solar spectral irradiance produced by the algorithm on 30<sup>th</sup> October 2003, when facular brightening and sunspot darkening values were relatively high.**

Quantity	Value and Uncertainty 121.5 nm	Value and Uncertainty 250.5 nm	Value and Uncertainty 500.5 nm	Value and Uncertainty 1000.5 nm
$c_F + c_S$	$(-1\pm 7)\times 10^{-8}$	$(2\pm 3)\times 10^{-6}$	$(-1\pm 0.9)\times 10^{-5}$	$(-9\pm 4)\times 10^{-6}$
$d_F$ Mg II index scalar	0.0047 $\pm$ 0.0001	0.095 $\pm$ 0.00001	0.18 $\pm$ 0.00002	0.055 $\pm$ 0.00002
$F(t)-F_Q$ MgII index change	0.0151 $\pm$ 0.003 (20%)	0.0151 $\pm$ 0.003 (20%)	0.0151 $\pm$ 0.003 (20%)	0.0151 $\pm$ 0.003 (20%)
$\Delta F(t)$ MgII index increment	0.0019 $\pm$ 0.0004	0.0019 $\pm$ 0.0004	0.0019 $\pm$ 0.0004	0.0019 $\pm$ 0.0004
$\Delta I_F(\lambda, t)$ facular SSI contribution	$(0.8\pm 0.2)\times 10^{-4}$ W m <sup>-2</sup> nm <sup>-1</sup>	$(1.6\pm 0.3)\times 10^{-3}$ W m <sup>-2</sup> nm <sup>-1</sup>	$(3.0\pm 0.6)\times 10^{-3}$ W m <sup>-2</sup> nm <sup>-1</sup>	$(9.4\pm 2)\times 10^{-4}$ W m <sup>-2</sup> nm <sup>-1</sup>
$d_S$ sunspot index scalar	$(3.68\pm 2545)\times 10^{-10}$	$(-2.9\pm 11)\times 10^{-8}$	$(-1.06\pm 0.2)\times 10^{-6}$	$(-2.05\pm 0.3)\times 10^{-7}$
$S(t)$ sunspot index change	10647 $\pm$ 2129 (20%)	10647 $\pm$ 2129 (20%)	10647 $\pm$ 2129 (20%)	10647 $\pm$ 2129 (20%)
$\Delta S(t)$ sunspot index increment	565 $\pm$ 113	565 $\pm$ 113	565 $\pm$ 113	565 $\pm$ 113
$\Delta I_S(\lambda, t)$ sunspot SSI contribution	$(4\pm 1)\times 10^{-6}$ W m <sup>-2</sup> nm <sup>-1</sup>	$(-3.28\pm 0.77)\times 10^{-4}$ W m <sup>-2</sup> nm <sup>-1</sup>	-0.012 $\pm$ 0.002 W m <sup>-2</sup> nm <sup>-1</sup>	-0.023 $\pm$ 0.005 W m <sup>-2</sup> nm <sup>-1</sup>
$I(\lambda, t) - I_Q(\lambda)$ SSI change	$(0.83\pm 0.18)\times 10^{-4}$ W m <sup>-2</sup> nm <sup>-1</sup>	0.0013 $\pm$ 0.0004 W m <sup>-2</sup> nm <sup>-1</sup>	-0.009 $\pm$ 0.003 W m <sup>-2</sup> nm <sup>-1</sup>	-0.0013 $\pm$ 0.0007 W m <sup>-2</sup> nm <sup>-1</sup>
$I_Q(\lambda)$	$(1.36\pm 0.14)\times 10^{-4}$ W m <sup>-2</sup> nm <sup>-1</sup> (10%)	0.0548 $\pm$ 0.003 W m <sup>-2</sup> nm <sup>-1</sup> (5%)	1.909 $\pm$ 0.1 W m <sup>-2</sup> nm <sup>-1</sup> (5%)	0.7422 $\pm$ 0.04 W m <sup>-2</sup> nm <sup>-1</sup> (5%)
$I(\lambda, t)$ absolute value	$(2.19\pm 0.17)\times 10^{-4}$ W m <sup>-2</sup> nm <sup>-1</sup>	0.0561 $\pm$ 0.0034 W m <sup>-2</sup> nm <sup>-1</sup>	1.900 $\pm$ 0.103 W m <sup>-2</sup> nm <sup>-1</sup>	0.7409 $\pm$ 0.0407 W m <sup>-2</sup> nm <sup>-1</sup>

## 5. Practical Considerations

### 5.1 Numerical Computation Considerations

The Solar Irradiance Climate Data Record algorithm uses basic algebra. There are no matrix inversions, extrapolations, or interpolations in the algorithm itself, which is computationally rapid, efficient and repeatable.

The Solar Irradiance Climate Data Record processing utilizes the LASP Time Series Server (LaTiS), an Application Programming Interface. This processing system accesses data files of sunspot area and location data of individual sunspot active regions present on the solar disk, archived at NOAA's National Geophysical Data Center (NGDC). An automated routine searches for new files daily and downloads files via ftp to LASP's Interactive Solar Irradiance Datacenter (LISIRD) for access by the NRLTSI2 and NRLSSI2 solar irradiance algorithms. New sunspot files are expected to occur roughly weekly with a latency of approximately 2 weeks. The latency is a result of the organization of the sunspot data files by sunspot group number (i.e. not by calendar date) and the time it takes a sunspot group to appear and then rotate off the solar disk. The processing system also operationally accesses the composite Mg II index record made by the GOME, SCIAMACHY and GOME-2 instruments using the same underlying LaTiS time series server.

The LaTiS provides user access to modeled solar irradiance data sets on LASP's LISIRD for a desired time range and for the desired variables. The Solar Irradiance Climate Data Record is provided to NOAA NCDC as NetCDF4 data files (Section 3.4.7).

### 5.2 Programming and Procedural Considerations

Execution speed is rapid and optimization is not needed. Given the facular and sunspot indices, the algorithm calculates the corresponding total and spectral irradiance in less than 2 seconds (on an iMac with Maverick Operating system).

### 5.3 Quality Assessment and Diagnostics

The quality assurance (QA) process utilizes both the science analysis and the data quality assurance. The Solar Irradiance Climate Data Record team oversees this process, which involves regular, careful examination of all solar and proxy data, and assesses the veracity and quality of the data to be released. The quality assurance takes several different forms based on: 1) the confidence in the calibration and performance of the instruments providing solar and proxy observations, 2) comparisons of model output with previous and simultaneous measurements, taking into account the calibration and performance of the direct, independent solar irradiance observations, and 3) understanding of the Sun and its variability – an understanding based on a broad range of solar models and on multiple solar observations at other wavelengths.

The Solar Irradiance Climate Data Record production system supports both automatic and manual diagnostic statistical analyses of the science products. Deviations from expected or predicted values, flagging of anomalous values, and trends of the sunspot blocking function and

facular brightening function, as well as final science values, are all incorporated into the assessment of the stability in the final science data products. The Solar Irradiance Data Record team will initially monitor the quality flags in the final science products manually. As the operational implementation of the Solar Irradiance Climate Data Record algorithm matures, the Solar Irradiance Data Record team will move toward automating portions of the quality flag in the final science products; manual monitoring, particularly of the physical representativeness of the facular brightening function and sunspot darkening function, will continue to be necessary to some extent.

A derived relationship between the Mg II index and the 10.7 cm radio flux ( $F_{10.7}$ , another proxy of chromospheric variability indicative of facular brightening, independent of the Mg II index) monitors, identifies, and flags outliers in the Mg II index value that is used to derive the facular brightening function relative to Quiet sun values. In addition, the time series of sunspot number is monitored to screen a value of '0' sunspot area as a "negative" result when the cause is missing station data, or a "positive" result when a value of '0' sunspot area is physically plausible at solar minimum conditions with zero sunspot number.

Statistical analyses of the time series of the mean facular brightening and sunspot darkening functions, and their respective variances, are used to flag potential outliers, alerting the Solar Irradiance Climate Data Record team to investigate the input data sets. The original NRLTSI and NRLSSI models provide robust data sets to define minimum and maximum ranges of the facular brightening and sunspot darkening functions. Statistical monitoring of the time series of the mean modeled solar irradiance (total and spectral), and their respective variances, is also implemented with near real-time comparisons with observations of total and spectral irradiance being made by *SORCE*, the TSI Transfer Calibration Experiment (TCTE), and the future TSIS instrument suite scheduled to launch to the International Space Station (ISS) in 2017.

Table 7 lists the assumptions in the algorithm. The operational steps to monitor time series of algorithm inputs and the output solar irradiance are also noted.

## 5.4 Exception Handling

The processing code is not currently robust when it comes to exception handling. Error conditions are unlikely, assuming the processing environment is adequately prepared. Future enhancements will ensure that appropriate error messages are returned.

## 5.5 Algorithm Validation

In addition to the checks on the algorithm performance described in Section 4, the algorithm is validated by comparing the total and solar spectral irradiance time series that it produces with direct observations where available, and with other models of irradiance variability.

Figures 14 and 15 compare the NRLTSI2 total irradiance time series with the observations made by *SORCE/TIM* and with the original NRLTSI model. NRLTSI2 captures 92% of the observed daily variability (correlation coefficient 0.96) and provides improved representation of *TIM* observations. The NRLTSI2 model-data residuals have a standard deviation of  $0.11 \text{ W m}^{-2}$

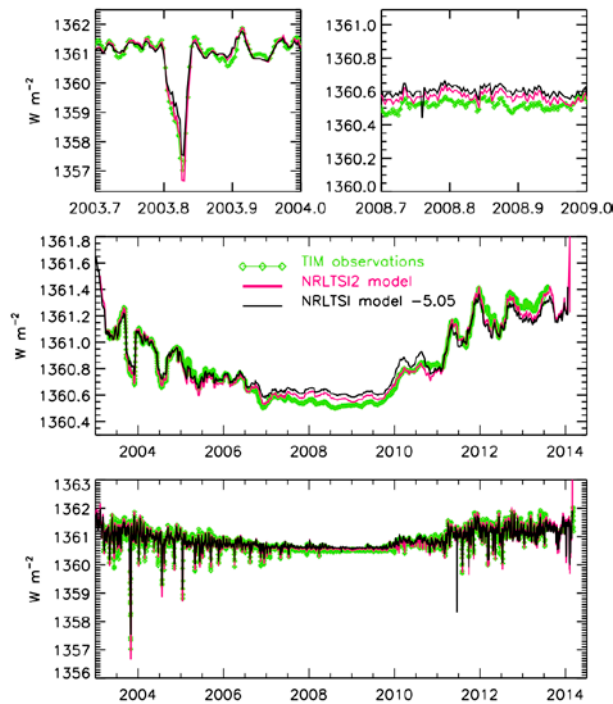


**Figure 14.** The total solar irradiance time series calculated by the algorithm (NRLTSI2 model) is compared with TIM observations during solar rotation (upper panel) and during the solar cycle (middle and lower panels). The middle panel is monthly-average data.

(compared with  $0.13 \text{ W m}^{-2}$  for NRLTSI) and a long-term trend of  $<2$  ppm per year (compared with 5 ppm per year for NRLTSI), which is less than TIM's 10 ppm long-term stability.

Figure 16 compares time series of solar spectral irradiance binned in selected broad wavelength bands, calculated by the NRLSSI2 model algorithm, compared with observations made by SORCE SIM and with equivalent time series of the NRLSSI model. The comparisons show spectral irradiance modulation associated with the Sun's 27-day rotation. On these relatively short (compared with the solar cycle) time scales, instrumental effects in the observations are assumed to be modest compared with true solar irradiance variability.

Actual solar cycle spectral irradiance changes are ambiguous because the only observations are those made by SIM on SORCE whose long-term stability has yet to be validated. Figure 17 shows solar cycle changes in spectral irradiance estimated by the NRLSSI2 algorithm, compared with the changes estimated by NRLSSI. Compared with NRLSSI, NRLSSI2 is more variable at wavelengths from 300 to 400 nm and less variability at wavelengths from 300 to 600 nm.

The Solar Irradiance Climate Data Record Team will continue to validate the solar irradiance CDR algorithm, with ongoing tests, statistical characterizations and self-consistency checks, and comparisons with observations. Planned for the immediate future are separate independent evaluations of the algorithms by both NRL and LASP, and regular comparisons and validation of the algorithm's operational products.

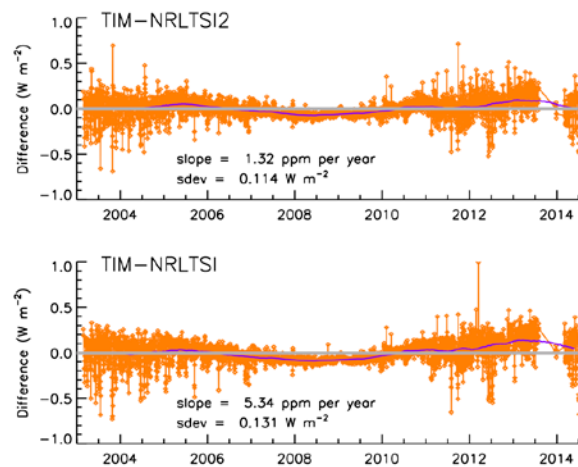


**Figure 15.** Differences in daily total solar irradiance that the algorithm calculates (according to NRLTSI2) with TIM observations (upper) and the original NRLTSI model (lower).

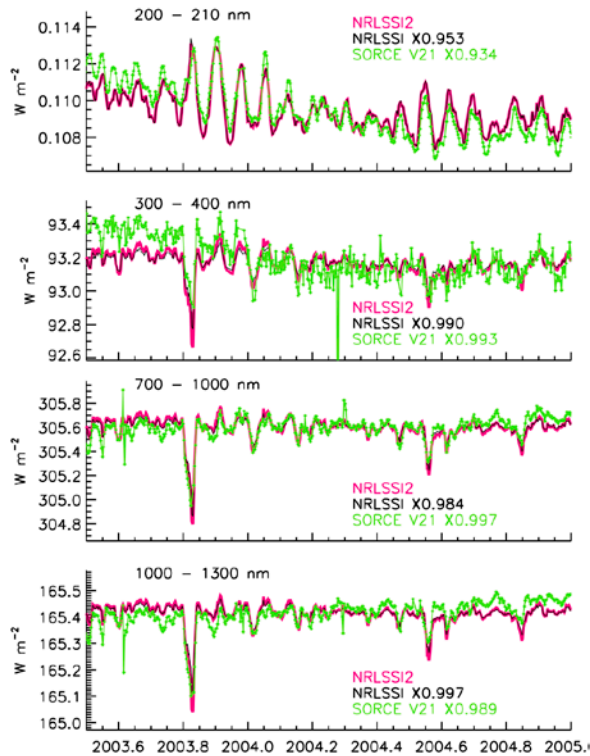


Figure 16. Shown are time series of solar spectral irradiance variations that the algorithm calculates (i.e., the NRLSSI2 model) and binned in broad wavelength bands compared with SIM observations from 2003 to 2005. The primary variations are associated with the Sun's 27-day rotation.

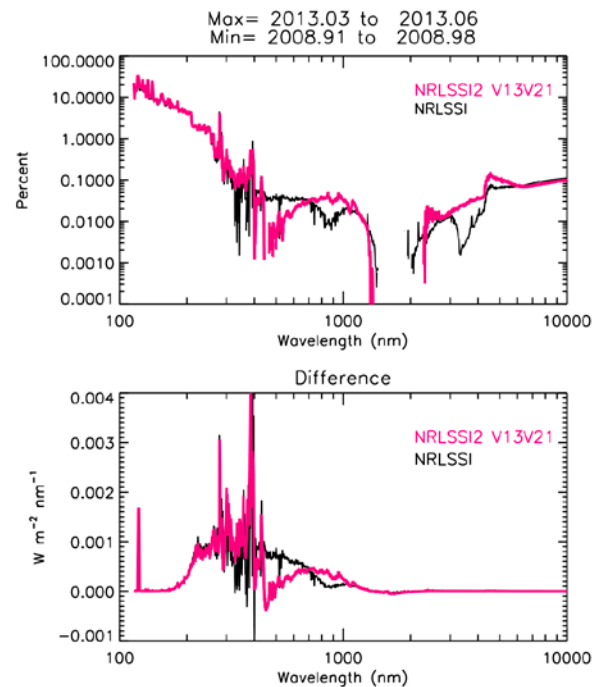


Figure 17. Shown are the solar spectral irradiance changes during solar cycle 24, in both percentages (upper) and energy units (lower), that the algorithm calculates (using the NRLSSI2 model) from solar minimum at the end of 2008 to near solar maximum at the beginning of 2013, compared with corresponding changes estimated using the original NRLSSI model.

## 5.6 Processing Environment and Resources

The processing code is written in IDL and requires version 8.2 or later. It runs on commodity hardware (e.g. 2 cores 8Gb RAM) with modest computation time, taking less than one minute to process one day. In principal the code could run on any OS with IDL, although it was developed on Unix-based systems. All the processing routines and utility routines are included in the code repository. The only (unlikely) storage concerns are for the final output products.

LaTiS, an Open Source software framework developed at LASP to provide uniform access to datasets, provides the primary data access layer. The sunspot area data from NGDC and the MgII index data on the SCIAMACHY scale from the University of Bremen are requested by the IDL processing code from a LaTiS server running at LASP. Other input files are included in the code repository and read directly by the IDL code.

## 6. Assumptions and Limitations

The assumptions in the algorithm's theoretical basis are detailed in Section 3. Table 7 summarizes these assumptions and the approach, where possible, to quantifying and monitoring their impacts on the modeled solar irradiance. The accuracy of the modeled solar irradiance also depends on the inputs (facular brightening and sunspot darkening indices) and the measurements used to derive these inputs (the Mg II index from UV solar spectrum observations and sunspot areas from white light solar imagery) have uncertainties themselves. In addition, there are uncertainties in the representativeness of the indices to the true (wavelength-dependent) facular brightening and sunspot darkening that produce irradiance changes. Also contributing to the uncertainty in the modeled irradiance, and possibly the easiest to quantify, are statistical uncertainties in the coefficients obtained by multiple regression of the input indices to the measured solar irradiance (total and spectral).

A number of validation studies have been performed, as illustrated in Section 5.5. The uncertainty estimates given in Tables 5 and 6 are initial first-time values that account for uncertainties in the input indices and in the multiple regression coefficients, and how these translate to equivalent irradiance uncertainties. But these initial estimates do not account for scientific assumptions in the algorithm. Work is ongoing to estimate more realistic uncertainties in the NRLTSI2 and NRLSSI2 modeled solar irradiances, by incorporating better quantification of the algorithm's assumptions, such as those that Table 7 identifies.

**Table 7. Summary of assumptions in the theoretical basis for modeled solar irradiance, model inputs and the potential validation approaches. Particular validation approaches that can be monitored over time (i.e. statistical) to provide an estimate in the uncertainty in the modeled solar irradiance are labeled 'Operational'.**

Assumptions & Scientific Support/Citation(s)	Validation Approach
Adopted value of the Quiet Sun (total and spectral) is invariant (Lean et al., 1998).	Comparison to irradiance measurements at solar minimum conditions.
Faculae brightening and sunspot darkening are the only modulators of <i>contemporary</i> solar irradiance and their respective impacts on irradiance are represented by linear adjustments of baseline, Quiet Sun, conditions (Lean et al., 1998, 2005; Lean, 2000; Lean and Woods, 2010).	<p>The derived facular and sunspot functions are imperfect indicators of the sunspot darkening and facular brightening sources. Small 'epsilon' regression coefficients correct for these differences.</p> <ul style="list-style-type: none"> <li>• <b>Operational:</b> Monitor the correlation between contemporary modeled and measured solar irradiance, and the standard deviation of residuals between modeled and measured solar irradiance.</li> <li>• Future improvements in the facular and sunspot functions may enable elimination of the small, but non-zero, correction coefficients.</li> </ul>
The background, facular brightening at <i>historical</i> , longer-term time scales (decade, centennial) is speculated (Lean et	A plausible magnitude of facular brightening is simulated from a flux-transport model that simulates eruption, transport, and accumulation of magnetic flux from

<p>al., 1992, 1995, 2000, 2002, 2005; Hoyt and Schatten, 1993; Tapping et al., 2007; Radick et al, 1998; Hall and Lockwood, 2004; Wang et al., 2005)</p>	<p>Maunder Minimum to present as a function proportional to sunspot number.</p> <ul style="list-style-type: none"> <li>• The effect is 27% lower than estimated in original NRLSSI model.</li> <li>• Monitor circumstantial evidence of facular impacts on irradiance trends: <ul style="list-style-type: none"> <li>○ Reduction in measured TSI corresponding with disappearance of faculae.</li> <li>○ Variations in chromospheric activity of Sun-like stars.</li> <li>○ Inferences with cosmogenic and geomagnetic indices.</li> <li>○ Inferences with changes in solar structure.</li> </ul> </li> </ul>
<p>The sunspot darkening function can be computed using sunspot areas, heliocentric locations, and number of individual sunspot regions (Allen, 1979; Lean et al., 1998; Brandt, Stix and Weinhart, 1994).</p> <ul style="list-style-type: none"> <li>• The relative contrast of sunspots to Quiet Sun irradiance is known with these assumptions: <ul style="list-style-type: none"> <li>○ The center-to-limb variation is independent of wavelength.</li> <li>○ Sunspot contrast is independent of position on solar disk and has an experimental bolometric (integrated) value of 0.32.</li> <li>○ Sunspot darkening function is the average of all sunspot areas and locations over the day.</li> </ul> </li> </ul>	<p>The solar rotation axis, ecliptic plane (beta angle) are known throughout the year and are used to adjust the projection of sunspot areas to the direction of the Earth, as it orbits the Sun.</p> <ul style="list-style-type: none"> <li>• Sunspot areas prior to 1976 are corrected for a systematic 20% high bias (measurement error).</li> <li>• <b>Operational:</b> Monitor mean and standard deviation of time series of sunspot darkening function.</li> <li>• <b>Operational:</b> Implement quality flags for the sunspot blocking function. Flag: <ul style="list-style-type: none"> <li>○ Missing station data</li> <li>○ Duplicate records</li> <li>○ Larger (or smaller) than expected variability.</li> </ul> </li> <li>• <b>Operational:</b> Monitor relationship between sunspot areas and sunspot number. If sunspot number is zero, a physically plausible result of sunspot area is 0 (i.e. “positive” result). If sunspot number is non-zero, a physically implausible result is a sunspot area of 0 (i.e. “negative” result).</li> </ul>
<p>The facular brightening function is a linear function of a flux “proxy” of facular brightening (Lean et al., 1998).</p> <ul style="list-style-type: none"> <li>• The Mg II index is a proxy for chromospheric variability, which is an extension of photospheric faculae (Snow et al., 2005).</li> <li>• The Mg II index is (relatively) free of instrumental sensitivity (drifts).</li> </ul>	<p>Faculae are poorly observed in solar imagery and inadequately specified.</p> <ul style="list-style-type: none"> <li>• <b>Operational:</b> Monitor mean and standard deviation of time series of facular brightening function. <ul style="list-style-type: none"> <li>○ For single, and multiple (i.e. overlapping in time) instruments.</li> </ul> </li> <li>• <b>Operational:</b> Monitor relationship between time series of Mg II index and the 10.7 cm radio flux. The relationship is expected to be consistent; a deviation is expected to be indicative of outlier in the Mg II record.</li> <li>• <b>Operational:</b> Implement quality flags for facular brightening based on Mg II record. Flag:</li> </ul>

	<ul style="list-style-type: none"> <li>○ Time gaps.</li> <li>○ Larger (or smaller) than expected variability.</li> <li>○ Outliers (when compared to F10.7 cm flux).</li> <li>● Future, reliable and quantitative, observations can be used to define statistical definitions of spectral irradiance changes due to faculae.</li> </ul>
<p>SORCE TIM measurements from 2003 to 2014 are the total solar irradiance standard used to compute scaling coefficients of facular brightening and sunspot darkening for NRLTSI2 using a multiple linear regression technique.</p> <ul style="list-style-type: none"> <li>● TSI of Quiet Sun is 1360.45 Wm<sup>-2</sup> (Kopp and Lean, 2011), based on SORCE TIM measured irradiance at solar minimum.</li> </ul>	<p><b>Operational:</b> Monitor the correlation between contemporary modeled and measured total solar irradiance, and the standard deviation of residuals between modeled and measured total solar irradiance.</p>
<p>SORCE SIM measurements contain instrumental trends (Lean and Deland, 2012).</p> <ul style="list-style-type: none"> <li>● Prior to application of multiple linear regression technique to observations, the SORCE SIM data is detrended (with 81 day running mean).</li> </ul>	<p>Compare wavelength-dependent scaling coefficients of facular brightening and sunspot darkening to their respective theoretical contrasts (ratio of emission to quiescent solar atmosphere).</p> <p>For <math>\lambda &gt; 290</math> nm: Use detrended TSI observations to determine the ratio of SSI multiple regression coefficients from direct observations to the detrended observations (i.e. an adjustment factor).</p> <p>For <math>\lambda &lt; 290</math> nm: Estimate adjustment to detrended multiple regression coefficients using Ca K time series; Ca K is a proxy of chromospheric variability independent of the Mg II index.</p>

The most probable cause of the algorithm generating incorrect irradiance values lies with the determination of the facular brightening and sunspot darkening indices, which rely on ground- and space-based observations of sunspot active regions and global facular brightness. The accuracy and precision of these ground-based observations is essentially unknown, and spurious inputs could produce unrealistic irradiance values. The algorithm flags input values that are deemed implausible, outside the range of current observed values.

Planned for future versions of the algorithms are more sophisticated near-real time validation of the sunspot darkening and facular brightening inputs that will aid in securing a more robust algorithm, e.g., comparisons of simultaneous calculations from independent databases.

## 6.1 Algorithm Performance

There are no assumptions made concerning algorithm performance. The algorithm is designed to compute modeled solar irradiance, using basic algebra, over a user-defined time range, and this input time range can be of arbitrary length. The algorithm is free of matrix inversions, parameter extrapolations or interpolations, and the execution is rapid and repeatable.

## 6.2 Sensor Performance

The solar irradiance reconstructions that this C-ATBD describes compliment the direct measurements of total and spectral solar irradiance made by the Total and Spectral Solar Irradiance Sensor (TSIS) instrument, documented in the TSIS ATBD (Coddington et al., 2013). The TSIS ATBD describes the algorithms used to produce all data levels of solar and spectral irradiance for the TSIS instrument complement, which consists of the Total Irradiance Monitor (TIM) and Spectral Irradiance Monitor (SIM). The TSIS ATBD also describes the predicted science and housekeeping operation modes, measurement error budgets, and the plan to monitor and correct for instrument degradation.

For solar irradiance, variations of less than 0.1% per decade are typical of the kinds of signals that must be extracted from “noisy” time-series measurements. The calibration approach adopted for TSIS characterizes the flight instrument as an “absolute sensor”. This involves characterizing each term in the measurement equation and tabulating a list of individual uncertainties and root sum square errors for overall measurement uncertainty.

### ***Accuracy and Long-term Stability of the TSIS Instrument Complement***

The TSIS TIM instrument is estimated to be three times more accurate than the SORCE TIM due to engineering advances in the optical and electrical sensors and to the end-to-end validation of the radiometer at the TSI Radiometer Facility (TRF) at the Laboratory for Atmospheric and Space Physics (LASP).

Lessons learned from the first-ever measurements of spectral solar irradiance made by the SORCE SIM have been incorporated into the TSIS SIM to meet the measurement requirements. Specific TSIS SIM capability improvements relative to SORCE SIM include reduced uncertainties in the prism degradation correction to meet long-term stability requirements, improved noise characteristics of the electrical substitution radiometer (ESR) and photodiode detectors to meet the measurement precision requirement, and improved absolute accuracy through pre-launch calibration using the novel, Spectral Radiometer Facility (SRF) at LASP.

The TSIS TIM will measure 4x daily total solar irradiance with an absolute accuracy of 100 ppm and a relative accuracy of 10 ppm per year. The TSIS SIM will measure 2x daily solar spectral irradiance at variable resolution from 200-2400 nm with an absolute accuracy of 0.2% (2000 ppm), a relative accuracy of 0.02% (200 ppm) and long-term relative stability of 0.05% per year (for wavelengths shortward of 400 nm) and 0.01% per year for wavelengths longward of 400 nm.

SORCE SIM data are currently being reanalyzed and its uncertainty estimates may change. It has been suggested that the SORCE SIM time series has not been fully corrected for instrument degradation and that the reported long-term (solar cycle) trends are not solely of solar origin (Lean and Deland, 2011). To reduce the sensitivity of the modeled solar spectral irradiance to these potential instrumental trends, the respective coefficients for sunspot darkening and facular brightening are derived from a multiple linear regression technique applied to the

sunspot area and Mg II index data, respectively, and the *detrended* (i.e. subtraction of an 81-day running mean) SORCE SIM observations (as described in Section 3.4).

### ***Degradation Monitoring and Correction of the TSIS Instrument Complement***

The sensitivities of all instruments on TSIS are assumed to degrade as the mission progresses and solar exposure accumulates. There are general assumptions that the degradation will monotonically decrease with time and that a primary cause of the decreased sensitivity is related to the exposure to the harsh radiation environment from the Sun. However, there is no guarantee these assumptions will be met and other changes that are strictly time-dependent, or aging effects, must also be considered. The possibility that instrument sensitivity may increase cannot be ruled out, and the degradation analysis does not preclude this condition.

Exposure and time-dependent degradation is a challenging problem and will require refinements throughout the mission as well as considerable analyses effort by the TSIS instrument scientists. In addition, any correction parameterization used initially may need evaluation and modification during the mission. Unexpected changes to the thermal stability of the spacecraft environment may require offsets in the analysis of certain data, and electronics and detector functionality can be impacted by energetic particles in major solar storms. Such impacts may require discontinuous changes in the science product rather than parameterized functions.

The Solar Irradiance Climate Data Record Team will maintain close contact with the TSIS instrument science team to secure robust understanding of observed long-term solar irradiance variations. The TSIS team will examine pre-launch characterizations and in-flight calibrations to derive appropriate degradation corrections to ensure the best available long-term observational record. The technique used to understand instrument degradation for the TSIS TIM and SIM instruments is to have completely independent instrument channels, to use each channel with a varying duty cycle, and then to compare their observations of the Sun. The degradation in the instruments is assumed to be primarily dependent on the exposure of the optics and detectors to solar radiation. With the assumption that exposure-dependent degradation will proceed proportionally faster for the normal channel, an exposure-dependent model of degradation is developed. The TSIS ATBD (Coddington et al., 2013) outlines a proposed model for monitoring and correcting each TSIS SIM observation for degradation.

## 7. Future Enhancements

Planned in the future are more sophisticated determinations, and near-real time validation, of the sunspot darkening and facular brightening inputs. Improved algorithm inputs will aid in securing more robust algorithm output. Also planned are improved uncertainty estimates, taking into account the assumptions in the algorithm formulation. On longer time scales, the algorithm may be revised and updated with a new formulation framework and coefficients, to reflect improved understanding of solar irradiance absolute scale and variability from ongoing analysis and recalibration of existing irradiance (and other) datasets, as well as the availability of reprocessed and new irradiance databases, such as from TCTE and TSIS observations.

Because solar irradiance is an essential, universal input for models of the terrestrial environment, we also anticipate provision of new irradiance products to accommodate the evolving needs of the user community, which we plan to monitor closely.

### 7.1 Enhancement 1: Improved Sunspot Darkening Index

Preliminary comparisons of the NRLTSI2 and NRLSSI2 models with observations suggest that improvements may be possible in the model's representations of the irradiance reduction due to the sunspot darkening. The comparison of the NRLTSI2 model with the TIM observations during the largest rotational modulation that *SORCE* has observed (in October 2003), shown in Figure 14 (upper left plot), suggests that NRLTSI2 overestimates slightly the total irradiance reduction at this time. This overestimation during times of large sunspot darkening is also evident in the comparison of the NRLSSI2 irradiance binned in broad wavelength bands with SIM observations, shown in Figure 16.

A likely reason for these differences is the less than optimal parameterization of the sunspot contrast with area. For example, Brandt et al. (1994) reported observational evidence for the dependence of sunspot contrast on sunspot area, according to

$$C_S^B - 1 = -[0.223 + 0.0244 \log_{10} A_S]$$

and this relationship was initially applied to the sunspot darkening function used to calculate the original NRLTSI and NRLSSI models. Preliminary studies suggest, however, that it worsens (slightly), rather than improves, the models' representations of the sunspot effect on irradiance. Future work is planned to investigate the dependence of sunspot contrast on area by calculating different sunspot darkening functions and evaluating their performance in the model formulation.

In the current algorithm, the sunspot darkening is calculated as the (unweighted) average of sunspot region information from ten different ground stations that contribute to the Air Force SOON program. We will investigate the robustness (repeatability and reliability) of the individual stations and consider a weighted average of their observations (also taking into account the local time of their observations, which alters the reported sunspot location on the disk) depending on the outcome of statistical comparisons. As well, different stations have different longevity within the record, with some stations terminating and some commencing at

different times. We will also investigate approaches for handling missing area data for a recorded sunspot group, as opposed to omitting the record from the average, such as replacing missing data with a weighted average value from other observing stations. For all of these analyses, we will compute the sunspot darkening function and evaluate how these differences translate into uncertainties in the input solar darkening index and hence in the solar irradiance that the algorithm outputs.

New, improved uncertainties in the sunspot darkening input to the algorithm will be estimated based on the results of the above analyses, as well as from comparisons with independent sunspot darkening calculations, such as in STARA (<http://www.nso.edu/staff/fwatson/STARA>) and from the Debrecen (<http://fenyi.solarobs.unideb.hu/DPD/>).

## 7.2 Enhancement 2: Improved Facular Brightening Index

Because the solar irradiance climate data record algorithm is formulated from multiple regression of the facular brightening and sunspot darkening indices with the TIM observations, changes in either index necessarily affect the proportion of irradiance variability that the model ascribes to each. An improved sunspot darkening index will therefore enable better assessment of limitations in the current facular index. We will investigate possible improvements to the facular index by analyzing the residuals of the observed irradiance and improved sunspot darkening indices (obtained from Enhancement 1, described above).

More problematic and challenging is securing a facular index that has robust long-term (solar cycle time scale) stability. There are distinct and reported differences among various Mg indices produced by different groups. In particular, changes from the successive 1996 to 2008 solar minima are not consistent (within current understanding) among various solar proxy indices (Snow et al., 2014). Analysis and study by the solar irradiance community is ongoing to secure the most reliable facular index possible. We will test the effect of new indices in the model formulation and algorithm, as well as compare different indices to better quantify irradiance uncertainties arising from this index.

As with the sunspot darkening analysis in Enhancement 1, future analysis of various facular brightening indices will enable improved uncertainties for this input to the algorithm.

## 7.3 Enhancement 3: Improved Uncertainty Estimates

Tables 5 and 6 provide estimates of uncertainties that the algorithm calculates in total solar irradiance and in solar spectral irradiance at selected wavelengths for one day (30<sup>th</sup> October 2003). Uncertainties in irradiance variability that the algorithm estimates vary with solar activity, which dramatically alters the magnitude of the sunspot darkening and facular brightening indices, as well as with wavelength, since the sunspot and facular contrasts have strong wavelength dependences. A future enhancement will expand and improve the uncertainty estimates in Tables 5 and 6, taking into account the improved quantitative estimates of uncertainties in solar irradiance arising from the sunspot darkening and facular brightening indices (described in Enhancements 1 and 2).

Most importantly, we plan to Investigate and attempt to quantify uncertainties arising from assumptions in the model formulation, such as those that Table 7 summarizes.

## **7.4 Enhancement 4: Improved Model Formulation**

The solar irradiance algorithm uses coefficients that require three databases for their determination: a time series of observed solar irradiance, a time series of the facular brightening index and a time series of sunspot darkening index. Significant (or even modest) changes in any of these time series may result in altered algorithm coefficients and warrant a new algorithm version. The sunspot and facular time series may change as a result of Enhancements 1 and 2, and the solar irradiance dataset may change as a result of reprocessing existing observations or by the addition of new observations.

It is possible that the current model formulation framework may also change in the longer-term future, to better reflect new understanding of the causes of solar irradiance variability, and taking into account the assumptions in Table 7. For example, the introduction of additional terms to the regression analysis would result in a new model formulation and CDR algorithm.

## **7.5 Enhancement 5: Additional Irradiance Products**

The current solar irradiance climate data record algorithm produces the solar spectral irradiance in 1 nm (or broader) spectral bands on a 1 nm (or broader) wavelength grid. However, fundamental, line-by-line calculations of atmospheric heating rates require the input solar spectral irradiance at higher spectral resolution and on a wavenumber grid. So a possible future additional irradiance product might be solar irradiance variability modeled on a higher resolution wavenumber grid.

## **7.6 Enhancement 6: Improved Exception Handling**

The processing code is not currently robust when it comes to exception handling. Error conditions are unlikely, assuming the processing environment is adequately prepared. Future enhancements will ensure that appropriate error messages are returned.

## **7.7 Enhancement 7: Improved Quality Flagging**

The current implementation of the data quality flag is immature. Future enhancements will implement a bit mask for multiple flags, improving the QA record to identify suspected outliers and duplicate or missing records in the input facular brightening and sunspot darkening indices, as well as outliers in the modeled total and spectral solar irradiance time series. The flagging of outliers in the input data will be assessed by comparison to independent but correlated data sets, such as the  $F_{10.7}$  time series, as well as known variability in the input data as derived from the original NRLTSI and NRLSSI models. The flagging of outliers in the modeled total and spectral solar irradiance will be based on comparisons to the measurement record.

As noted in Sections 5.3 and 6, initial manual monitoring by the Solar Irradiance Data Record, particularly of the input data sets, will ultimately lead to improved operational implementation of the Solar Irradiance Climate Data Record algorithm and confidence in the quality flagging.

## 8. References

- Allen, C. W. 1981, *Astrophysical Quantities* (3d ed.; London : Athlone)
- Brandt, P. N., M. Stix, M., and H. Weinhardt (1994). Modelling solar irradiance variations with an area dependent photometric sunspot index. *Solar Phys.* 152:119-124.
- Coddington, O., P. Pilewskie, E. Richard, G. Kopp, J. Lean, D. Harber, E. Hartnett, and S. Beland (2013). TSIS Algorithm Theoretical Basis Document (ATBD) (*draft*).
- Fröhlich, C., and J. Lean (2004). Solar irradiance variability and climate. *Astron. Astrophys. Rev.*, 12 (4), 273-320, doi: 10.1007/s00159-004-0024-1
- Hall, J. C. and G. W. Lockwood (2004). The Chromospheric Activity and Variability of Cycling and Flat Activity Solar-Analog Stars. *Astrophys. J.*, 614:942, doi:10.1086/423926.
- Hoyt, D. V., and K. H Schatten (1993). A discussion of plausible solar irradiance variations, 1700-1992. *J. Geophys. Res.*, 98.A11: 18895-18906.
- Kopp, G., and J. L. Lean (2011). A new low value of Total Solar Irradiance: evidence and climate significance. *Geophys. Res. Lett.*, 38, L01706, doi:10.1029/2010GL045777 2011
- Kurucz, R.L. (1991). The solar spectrum. *The University of Arizona Press, Tucson*, pp. 663-669.
- Lean, J., A. Skumanich, and O. R. White (1992). Estimating the Sun's Radiative Output During the Maunder Minimum. *Geophys. Res. Lett.*, 19:1591-1495.
- Lean, J., J. Beer, and R. Bradley (1995). Reconstruction of solar irradiance since 1610: Implications for climate change. *Geophys. Res. Lett.*, 22:3195-3198.
- Lean, J. L., G. J. Rottman, H. L. Kyle, T. N. Woods, J. R. Hickey, and L. C. Puga (1997). Detection and parameterization of variations in solar mid and near ultraviolet radiation (200 to 400 nm). *J. Geophys. Res.*, 102:29939-29956.
- Lean, J. L., J. Cook, W. Marquette, and A. Johannesson (1998). Magnetic modulation of the solar irradiance cycle. *Astrophys. J.*, 492: 390-401.
- Lean, J. L., O. R. White, W. C. Livingston, and J. M. Picone (2001) Variability of a composite chromospheric irradiance index during the 11-year activity cycle and over longer time period. *J. Geophys. Res.*, 106, 10,645-10,658.
- Lean, Judith (2000). Evolution of the Sun's Spectral Irradiance since the Maunder Minimum. *Geophys. Res. Lett.*, 27:2425-2428.
- Lean, J., G. Rottman, J. Harder, and G. Kopp (2005). *SORCE* contributions to new understanding of global change and solar variability. *Solar Phys.*, 230, 27-53, DOI: 10.1007/s11207-005-1527-2
- Lean, J., Y.-M. Wang, and N. R. Sheeley, Jr. (2002). The effect of increasing solar activity on the Sun's total and open magnetic flux during multiple cycles; Implications for solar forcing of climate. *Geophys. Res. Lett.*, 29, doi:10.1029/2002GL015880.

- Lean, J. L., and T. N. Woods (2010). Solar spectral irradiance measurements and models, in *Evolving Solar Physics and the Climates of Earth and Space*, Karel Schrijver and George Siscoe (Eds), Cambridge Univ. Press.
- Lean, J. L., T. N. Woods, F. Eparvier, R. R. Meier and D. J. Strickland, Solar EUV Irradiance, Past, Present and Future (2011). *J. Geophys. Res.*, 116, A01102, doi:10.1029/2010JA015901.
- Lean, J. L., and M. T. Deland (2012). How does the Sun's spectrum vary? *J. Climate*, 25: 2555-2560, doi: <http://dx.doi.org/10.1175/JCLI-D-11-00571.1>.
- Radick, R. R., G. W. Lockwood, B. A. Skiff, and S. L. Baliunas (1998) Patterns of Variation among Sun-like Stars. *Astrophys. J. Suppl.* 118:239 doi:10.1086/313135.
- Rottman, G. J. (2000). Variations of solar ultraviolet irradiance observed by the UARS SOLSTICE — 1991 to 1999. *Space Sci. Rev.*, 94 (1-2), 83-91, DOI: 10.1023/A:1026786315718.
- Rottman, G. J., J. Harder, J. Fontenla, T. Woods, O. R. White and G. M. Lawrence (2005). The Spectral Irradiance Monitor (SIM): Early observations. *Solar Phys.*, 230:7-25, DOI: 10.1007/s11207-005-8112-6.
- Schmidt, G. A., J. H. Jungclaus, C. M. Ammann, E. Bard, P. Braconnot, T. J. Crowley, G. Delaygue, F. Joos, N. A. Krivova, R. Muscheler, B. L. Otto-Bliesner, J. Pongratz<sup>1</sup>, D. T. Shindell, S. K. Solanki, F. Steinhilber, and L. E. A. Vieira ( 2011). Climate forcing reconstructions for use in PMIP simulations of the last millennium (v1.0). *Geosci. Model Dev.*, 4:33–45, doi:10.5194/gmd-4-33-2011.
- Skupin, J., M. Weber, H. Bovensmann, and J. P. Burrows (2004). The Mg II solar activity proxy indicator derived from GOME and SCIAMACHY. *Proceedings of the ENVISAT & ERS Symposium (SP-572)*, ESA Publications Division.
- Snow, M., W. E. McClintock, T. N. Woods, O. R. White, J. W. Harder, and G. Rottman (2005). The Mg II Index from SORCE, *Solar Phys.*, 230:325-344.
- Snow, M. J., M. Weber, J. Machol, R. Viereck, and E. Richard (2014). Comparison of Magnesium II core-to-wing ratio observations during solar minimum 23/24. *Space Weather Space Clim.* 4:A04, <http://dx.doi.org/10.1051/swsc/2014001>.
- Tapping, K. F., D. Boteler, P. Charbonneau, A. Crouch, A. Manson, and H. Paquette (2007). Solar magnetic activity and total irradiance since the Maunder Minimum. *Sol. Phys.*, 246,:309–326, doi:10.1007/s112070079047x.
- Thuillier, G., M. Hersé, P. C. Simon, D. Labs, H. Mandel, D. Gillotay, and T. Foujols (1998). The visible solar spectral irradiance from 350 to 850 nm as measured by the SOLSPEC spectrometer during the ATLAS I mission. *Solar Phys.*, 177:41-61.
- Thuillier, G., Melo, S. M. L., Lean, J. L., Krivova, N. A., Bolduc, C., Fomichev, V. I., Charbonneau, P., Shapiro, A. I., Schmutz, W., and Bolsée, D. (2013). Analysis of Different Solar Spectral Irradiance Reconstructions and Their Impact on Solar Heating Rates. *Solar Phys.*, DOI 10.1007/s11207-013-0381-x.

- Unruh, Y.C., S. K. Solanki, and M. Fligge (2000). Modelling solar irradiance variations: Comparison with observations, including line-ratio variations. *Space Sci. Rev.*, 94 (1-2):145-152, DOI: 10.1023/A:1026758904332.
- Wang, Y.-M., J. L. Lean, and N. R. Sheeley, Jr. (2005). Modeling the Sun's magnetic field and irradiance since 1713. *Astrophys. J.*, 625:522–538.
- Woods, T. N., P. C. Chamberlin, J. W. Harder, R. A. Hock, M. Snow, F. G. Eparvier, J. Fontenla, W. E. McClintock, and E. C. Richard (2009). Solar irradiance reference Spectra (SIRS) for the 2008 Whole Heliosphere Interval (WHI), *Geophys. Res. Lett.*, 36, L01101, doi:10.1029/2008GL036373.

## Appendix A. Acronyms and Abbreviations

Acronym or Abbreviation	Meaning
$\lambda$	Lambda; wavelength (nm)
$\mu$	Heliographic position
ACRIM	Active Cavity Radiometer Irradiance Monitor
C-ATBD	Climate Algorithm Theoretical Basis Document
Ca K	Calcium K Fraunhofer line in the solar spectrum
CDR	Climate Data Record
F(t)	Facular Brightening Function (time-dependent)
F10.7	Solar radio flux at 10.7 cm
GOME	Global Ozone Monitoring Experiment
GOME-2	Global Ozone Monitoring Experiment 2
I(t)	Solar Spectral Irradiance (time-dependent)
$I_{\odot}$	Solar Spectral Irradiance of the Quiet Sun
ISS	International Space Station
LASP	Laboratory for Atmospheric and Space Physics
LaTiS	LASP Time Series Server
LISIRD	LASP Interactive Solar Irradiance Data Center
m	meter
Mg II	Magnesium II index
MDI	Michelson Doppler Imager
NCDC	National Climatic Data Center
netCDF4	Network Common Data Format
NIMBUS	Series of NASA satellites, first launched in 1964; NIMBUS-7 was the last in the series.
NOAA	National Oceanographic and Atmospheric Administration
NGDC	NOAA National Geophysical Data Center
NRL	Naval Research Laboratory
NRLSSI	Naval Research Laboratory Solar Spectral Irradiance model (original)
NRLSSI2	Naval Research Laboratory Solar Spectral Irradiance model (version 2, this C-ATBD)
NRLTSI	Naval Research Laboratory Total Solar Irradiance model (original)

NRLTSI2	Naval Research Laboratory Total Solar Irradiance model (version 2, this C-ATBD)
nm	nanometer
NOAA	National Oceanic and Atmospheric Administration
PMOD	Physikalisch-Meteorologisches Observatorium Davos
ppm	Part per million
QA	Quality Assurance (Analysis)
R	Radiance
S(t)	Sunspot Darkening Function (time-dependent)
SCIAMACHY	Scanning Imaging Absorption SpectroMeter for Atmospheric ChartographY
SIM	Spectral Irradiance Monitor
SMM	Solar Maximum Mission
SOHO	Solar and Heliospheric Observatory
SOLSPEC	SOLar SPECTral Irradiance Measurements; French instrument that measured irradiance from the ISS
SOLSTICE	Solar Stellar Intercomparison Experiment
SOON	Solar Observing Optical Network (US Air Force)
SORCE	Solar Radiation and Climate Experiment
SRF	Spectral Radiometer Facility (LASP)
SSD	Space Science Division (Naval Research Laboratory, Washington, DC)
SSI	Solar Spectral Irradiance
STARA	Sunspot Tracking and Recognition Algorithm
T(t)	Total Solar Irradiance (time-dependent)
T <sub>Q</sub>	Total Solar Irradiance of the Quiet Sun
TCTE	TSI Transfer Calibration Experiment
TIM	Total Irradiance Monitor
TRF	TSI Radiometer Facility (LASP)
TSI	Total Solar Irradiance
TSIS	Total and Spectral Solar Irradiance Sensor
UARS	Upper Atmosphere Research Satellite
USAF_MWL	US Air Force Mount Wilson Observatory
UV	ultraviolet
W	Watt